American Mineralogist, Volume 76, pages 827–847, 1991

Chromian spinels as petrogenetic indicators: Thermodynamics and petrological applications

RICHARD O. SACK
Department of Earth and Atmospheric Sciences, Purdue University, West Lafayette, Indiana 47907, U.S.A.
MARK S. GHIORSO
Department of Geological Sciences, AJ-20, University of Washington, Seattle, Washington 98195, U.S.A.

ABSTRACT

A model is developed for the thermodynamic properties of chromian spinels of petrological interest. It is formulated for the simplifying assumptions that (1) cations exhibit only long-range, nonconvergent ordering between tetrahedral and octahedral sites and that (2) the vibrational Gibbs energy may be described by a Taylor expansion of only second degree for seven linearly independent variables of composition and ordering. The model is calibrated using (1) the partitioning relations of Mg and Fe between spinels and olivine, (2) the distribution coefficients for the exchange of Al and Cr between spinels and $(Al,Cr)_2O_3$ solid solutions, (3) the features of the miscibility gaps in chromium titanium aluminum spinels, (4) the activity composition data in the chromite-magnetite subsystem, and (5) the constraints of cation site ordering. It is consistent with the observations summarized by Sack and Ghiorso (1991) for Cr-free spinels. The calibration is achieved with the further simplifying assumption that all thermodynamic parameters corresponding to second-degree Taylor coefficients are constants independent of temperature (i.e., there are no excess vibrational entropies of mixing).

The proposed model is internally consistent with the thermodynamic data of Berman (1988) and our previous analyses of the solution properties of olivine, orthopyroxene, and rhombohedral oxides (Sack and Ghiorso, 1989; Ghiorso, 1990a). We develop a geothermometer based on the exchange of Mg and Fe between olivine and spinel that may be applied with confidence to assemblages that formed at low pressures and at temperatures between 400 and 1400 °C. We utilize this geothermometer to define equilibration temperatures for subassemblages of olivine + spinel in metamorphosed ultramafic rocks of the greenschist-amphibolite facies. Phase relations within the spinel prism $[(Fe,Mg)(Al,Cr,Fe^{3+})_2O_4]$ are calculated for temperatures over the range 500–600 °C and compare favorably with petrologic observations.

INTRODUCTION

Cr is an essential constituent of many spinels in mafic-ultramafic igneous and metamorphic rocks of the crust and upper mantle. Although they are typically only accessory phases, such spinels have been widely recognized as potentially important petrogenetic indicators (e.g., Irvine, 1965, 1967; Evans and Frost, 1975; Sack, 1982; Engi, 1983). For example, the Cr contents of homogeneous spinels provide a sensitive indicator of the degree of fractionation and of interactions between host liquids and wall rocks for the MORB-type basalts of the Lamont seamount chain (Allan et al., 1988, 1989). Chromian spinels exhibit complex patterns of chemical zoning that may be used to monitor changes in the compositions of both melt and solid phases during crystallization of basaltic liquids (e.g., El Goresy, 1976). Chromian spinels have also been utilized to track the evolution of the fluid phase during regional metamorphism of serpentinites (e.g., Hoffman and Walker, 1978). To interpret quantitatively such features, it is necessary to develop a thermodynamic model for chromian spinels.

In this paper we update and extend our analysis of the thermodynamic properties of $(Fe,Mg)(Al,Fe^{3+})_2O_4$-$(Fe,Mg)_2TiO_4$ (Sack and Ghiorso, 1991) to Cr-bearing systems. This effort is part of an ongoing program to develop internally consistent thermodynamic data for standard state and mixing properties of the common rock-forming minerals (e.g., Berman, 1988; Sack and Ghiorso, 1989, 1991; Ghiorso, 1990a; Ghiorso and Sack, 1991). Here we calibrate a model for the thermodynamic properties of chromian spinels based upon (1) high temperature activity-composition data for $FeCr_2O_4$-Fe_3O_4 (Katsura et al., 1975; Petric and Jacob, 1982a), (2) experimental constraints on Cr-Al partitioning between $(Al,Cr)_2O_3$ and $Fe(Al,Cr)_2O_4$, $(Al,Cr)_2O_3$ and $Mg(Al,Cr)_2O_4$, and $Na(Al,Cr)Si_2O_6$ and $Mg(Al,Cr)_2O_4$ (Petric and Jacob, 1982b; Oka et al., 1984; Carroll Webb and Wood, 1986), (3) features of miscibility gaps in $FeAl_2O_4$-Fe_2TiO_4-$FeCr_2O_4$ and $MgAl_2O_4$-Mg_2TiO_4-$MgCr_2O_4$ (Muan et al.,

0003–004X/91/0506–0827$02.00

1972), and (4) both experimental and petrological constraints on Fe-Mg partitioning between olivine and chromian spinels (Sack, 1982; Engi, 1983; Murck and Campbell, 1986; Allan et al., 1987, 1988). A calibration of a geothermometer based on the exchange of Mg and Fe between olivine and spinel is compared with constraints from petrological studies of metamorphosed ultramafic rocks (e.g., Muir and Naldrett, 1973; Evans and Frost, 1975; Hoffman and Walker, 1978; Loferski and Lipin, 1983; Zakrzewski, 1989), and some unusual features of the results are noted. To clarify phase relations in the spinel prism (e.g., Irvine, 1965) under conditions appropriate for the greenschist-amphibolite facies of metamorphism, we present and analyze isothermal sections for $(Fe,Mg)(Al,Fe^{3+},Cr)_2O_4$ in equilibrium with Fo_0, Fo_{60}, Fo_{80}, Fo_{90}, Fo_{95}, and Fo_{100} olivine over the temperature range 500–600 °C.

Thermodynamics

A thermodynamic model for chromian spinels may be readily developed by extension of the model of Sack and Ghiorso (1991) for $(Fe,Mg)(Al,Fe^{3+})_2O_4$-$(Fe,Mg)_2TiO_4$. In the formulation of Sack and Ghiorso it is assumed that all spinels exhibit R_3O_4 stoichiometry, with $Fd3m$ space group symmetry. It is further assumed that they do not exhibit short-range cation ordering and that Ti^{4+} occupies only octahedral sites. The molar Gibbs energy ($\bar{G}$) is given by the equation

$$\bar{G} = \bar{G}^* - T\bar{S}^{IC} \tag{1}$$

where $\bar{G}^*$ is the vibrational Gibbs energy and $\bar{S}^{IC}$ is the ideal molar configurational entropy. The molar vibrational Gibbs energy, $\bar{G}^*$, is described using a Taylor expansion of second degree in composition (X_i) and ordering variables (s_i) (cf. Thompson, 1969)

$$\bar{G}^* = g_o + \sum_i \left(g_i X_i + g_{ii} X_i^2 + \sum_{j<i} g_{ij} X_i X_j \right) + \sum_i \sum_k (g_{ik} X_i s_k) + \sum_k \left(g_k s_k + g_{kk} s_k^2 + \sum_{l<k} g_{kl} s_k s_l \right). \tag{2}$$

The expression for the configurational entropy is deduced by substituting into the relation

$$\bar{S}^{IC} = -R \sum_r \sum_c \bar{r} X_{c,r} \ln X_{c,r} \tag{3}$$

expressions that define the mole fractions of cations on sites ($X_{c,r}$) in terms of the composition (X_i) and ordering (s_i) variables. In Equation 3, $\bar{r}$ is the number of sites of type r per formula unit, $X_{c,r}$ refers to the cation fraction of c on site r, and R is the universal gas constant. Expressions for the chemical potentials of spinel components are derived from the expression for $\bar{G}$ by application of an extended form of the so-called Darken equation (Darken and Gurry, 1953; Sack, 1982; Sack et al., 1987a; Ghiorso, 1990b)

$$\mu_j = \bar{G} + \sum_i n_{ij}(1 - X_i)(\partial \bar{G}/\partial X_i)_{X_{k/X_l,s_m}} + \sum_i (q_{ij} - s_i)(\partial \bar{G}/\partial s_i)_{X_k,s_l} \tag{4}$$

where n_{ij} and q_{ij} refer to the values of X_i and s_i, respectively, in 1 mol of spinel component j. The order variables are evaluated by setting the derivatives $(\partial \bar{G}/\partial s_i)$ successively equal to zero.

Thermodynamic parameters of the formulation of Sack and Ghiorso (1991) that correspond with coefficients of the Taylor expansion are of six types: (1) vibrational Gibbs energies of end-members with inverse structural states [$\bar{G}_1^*$ ($FeAl_2O_4$), $\bar{G}_2^*$ ($MgAl_2O_4$), $\bar{G}_4^*$ (Fe_2TiO_4), and $\bar{G}_5^*$ (Fe_3O_4), (2) differences in vibrational Gibbs energies between normal and inverse 2-3 spinel end-members ($\Delta\bar{G}^*_{1'1}$, $\Delta\bar{G}^*_{5'5}$, where the normal state is denoted by a primed superscript), (3) standard state Gibbs energies of the reciprocal reactions for Mg and Fe between aluminate and titanate ($\Delta\bar{G}^0_{24}$), and between aluminate and ferrite ($\Delta\bar{G}^0_{25}$) spinels with inverse cation distributions, (4) standard state Gibbs energies of the reciprocal-ordering and exchange reactions in titanate spinels ($\Delta\bar{G}^0_X$ and $\Delta\bar{G}^0_{EX}$), (5) symmetric regular-solution-type parameters describing departures from linearity in vibrational Gibbs energy along joins between normal and inverse 2-3 end-member spinels ($W_{1'1}$, $W_{2'2}$, and $W_{5'5}$), and (6) symmetric regular-solution-type parameters describing departures from linearity in vibrational Gibbs energy along joins between vertices differing in composition ($^{[4]}W_{FeMg}$, $^{[6]}W_{FeMg}$, W_{14}, $W_{1'4}$, W_{15}, $W_{1'5}$, $W_{15'}$, $W_{1'5'}$, W_{24}, $W_{2'4}$, $W_{2'5}$, $W_{25'}$, W_{45}, $W_{45'}$ and $W_{45'}$, where the underscore refers to the magnesian rather than the Fe^{2+} end-member component). Some inferred relations between thermodynamic parameters are a consequence of the assumption that the vibrational Gibbs energy is only a second-degree function of composition and ordering variables (i.e., no ternary terms are required). To accommodate these, Sack and Ghiorso (1991) made the simplifying assumption that there is no excess vibrational entropy of mixing. This implies that all homogeneous reactions have constant vibrational Gibbs energies and that all regular-solution-type parameters are constants independent of temperature. With the minor adjustments outlined herein the model of Sack and Ghiorso (1991) successfully accounts for cation ordering constraints, the composition and temperature dependence of distribution coefficients for Fe and Mg exchange between spinels and olivines, features of miscibility gaps, activity-composition data, and calorimetric constraints on standard state properties of end-member components.

To extend the formulation of Sack and Ghiorso (1991) to Cr-bearing spinels, we define the following composition and ordering variables

$$X_3 \equiv {}^{[4]}X_{Cr^{3+}} + 2^{[6]}X_{Cr^{3+}}$$

and

$$s_3 \equiv \tfrac{1}{2}[2\,{}^{[6]}X_{Cr^{3+}} - {}^{[4]}X_{Cr^{3+}}].$$

Inclusion of these definitions results in the following set of linearly independent composition variables for the extended system:

$$X_2 = {}^{[4]}X_{Mg^{2+}} + 2^{[6]}X_{Mg^{2+}} \quad (5a)$$
$$X_3 = {}^{[4]}X_{Cr^{3+}} + 2^{[6]}X_{Cr^{3+}} \quad (5b)$$
$$X_4 = 2^{[6]}X_{Ti^{4+}} \quad (5c)$$

and

$$X_5 = {}^{[4]}X_{Fe^{3+}} + 2^{[6]}X_{Fe^{3+}} \quad (5d)$$

and the following set of ordering variables:

$$s_1 = {}^{[4]}X_{Mg^{2+}} - 2^{[6]}X_{Mg^{2+}} \quad (6a)$$
$$s_2 = \tfrac{1}{2}[2^{[6]}X_{Al^{3+}} - {}^{[4]}X_{Al^{3+}}] \quad (6b)$$
$$s_3 = \tfrac{1}{2}[2^{[6]}X_{Cr^{3+}} - {}^{[4]}X_{Cr^{3+}}] \quad (6c)$$

and

$$s_4 = \tfrac{1}{2}[2^{[6]}X_{Fe^{3+}} - {}^{[4]}X_{Fe^{3+}}]. \quad (6d)$$

Given the site population constraints provided by

$$1 = {}^{[4]}X_{Fe^{2+}} + {}^{[4]}X_{Mg^{2+}} + {}^{[4]}X_{Al^{3+}} + {}^{[4]}X_{Cr^{3+}} + {}^{[4]}X_{Fe^{3+}} \quad (7a)$$

and

$$1 = {}^{[6]}X_{Fe^{2+}} + {}^{[6]}X_{Mg^{2+}} + {}^{[6]}X_{Al^{3+}} + {}^{[6]}X_{Cr^{3+}} + {}^{[6]}X_{Fe^{3+}} + {}^{[6]}X_{Ti^{4+}} \quad (7b)$$

we may readily derive expressions that relate the mole fractions of cations on tetrahedral and octahedral sites to these composition and ordering variables. The resulting definitions of site mole fractions are provided in Table 1. We next adopt a linearly independent set of thermodynamic parameters, analogous to those employed by Sack and Ghiorso (1991), and identify these with coefficients of the Taylor expansion. Substitution of these identities into Equation 2 generates an explicit expression for the molar vibrational Gibbs energy. Some simplification is achieved by setting the ordering variable s_3 to equal the composition variable X_3, in accordance with the observation that Cr^{3+} has an extremely strong preference for octahedral relative to tetrahedral sites (e.g., Dunitz and Orgel, 1957; Navrotsky and Kleppa, 1967). Our adopted set of thermodynamic parameters reflects this simplification and is provided in Table 2. The resulting expression for the molar Gibbs energy is given in Table 3. Before proceeding with the analysis, we define two linearly dependent thermodynamic parameters that emerge from truncating the expansion for $\overline{G}^*$ at second degree

$$W_{\underline{3'5}} = W_{3'5} + (W_{\underline{23'}} + W_{2'\underline{5}} + W_{1'1}) - (W_{13'} + W_{1'5} + W_{2'2}) \quad (8)$$

and

TABLE 1. Definitions of site mole fractions

${}^{[4]}X_{Mg^{2+}}$	$\frac{X_2 + s_1}{2}$
${}^{[4]}X_{Fe^{2+}}$	$X_4 + s_2 + s_3 + s_4 - \frac{X_2 + s_1}{2}$
${}^{[4]}X_{Fe^{3+}}$	$X_5 - s_4$
${}^{[4]}X_{Al^{3+}}$	$1 - X_3 - X_4 - X_5 - s_2$
${}^{[4]}X_{Cr^{3+}}$	$X_3 - s_3$
${}^{[6]}X_{Mg^{2+}}$	$\frac{X_2 - s_1}{4}$
${}^{[6]}X_{Fe^{2+}}$	$\frac{1 - s_2 - s_3 - s_4}{2} - \frac{X_2 - s_1}{4}$
${}^{[6]}X_{Fe^{3+}}$	$\frac{X_5 + s_4}{2}$
${}^{[6]}X_{Al^{3+}}$	$\frac{1 - X_3 - X_4 - X_5 + s_2}{2}$
${}^{[6]}X_{Cr^{3+}}$	$\frac{X_3 + s_3}{2}$
${}^{[6]}X_{Ti^{4+}}$	$\frac{X_4}{2}$

$$\Delta\overline{G}^{0(N)}_{23} = (W_{\underline{3'4}} - W_{3'4}) + (W_{13'} - W_{\underline{23'}}) + (W_{2'2} - W_{1'1}) + (W_{1'4} - W_{2'\underline{4}}). \quad (9)$$

$W_{3'5}$ refers to the regular-solution-type parameter describing deviations from linearity in the vibrational Gibbs energy along the join $Mg(Cr)_2O_4$-$Fe(Mg,Fe)_2O_4$. The term $\Delta\overline{G}^{0(N)}_{23}$ is the standard state Gibbs energy of the reaction

$$Fe(Cr)_2O_4 + Mg(Al)_2O_4 = Fe(Al)_2O_4 + Mg(Cr)_2O_4$$

where the parentheses denote octahedral sites. An exhaustive list of additional dependent parameters for the chromium absent system is provided in Table 6 of Sack and Ghiorso (1991).

Calibration for Cr-bearing spinels

Before proceeding with our analysis of chromian spinels, some adjustments to the calibration of Sack and Ghiorso (1991) are required. In our earlier calibration for the energetic parameters of $MgAl_2O_4$ ($\Delta\overline{H}^*_{2'2}$ and $W_{2'2}$), we relied upon constraints on the degree of order (s_2) for Al and Mg between tetrahedral and octahedral sites at high temperatures obtained by Wood et al. (1986). These authors used ^{27}Al magic angle spinning (MAS) nuclear magnetic resonance (NMR) spectroscopy to characterize synthetic samples annealed over the temperature range 700–1000 °C. However, it has been demonstrated in a subsequent MAS-NMR reexamination of similar samples (Millard et al., in preparation) that Wood et al. (1986) overestimated the degree of Al-Mg disorder because they employed a B_1 pulse length that is problematic at the magnetic field intensities employed during their spectra acquisition. Results of Millard et al. (in preparation) and

TABLE 2. Linearly independent thermodynamic parameters

	Parameter type	
	Label	Definition
End-member components	$\overline{G}^*_1$	$\overline{G}^*_{Al(Al,Fe)_2O_4}$
	$\overline{G}^*_2$	$\overline{G}^*_{Al(Al,Mg)_2O_4}$
	$\overline{G}^*_3$	$\overline{G}^*_{Cr(Fe^{2+},Cr)_2O_4}$
	$\overline{G}^*_4$	$\overline{G}^*_{Fe(Fe,Ti)_2O_4}$
	$\overline{G}^*_5$	$\overline{G}^*_{Fe^{3+}(Fe^{2+},Fe^{3+})_2O_4}$
Ordering energies in 2–3 spinels	$\Delta\overline{G}^*_{1'1}$	$\overline{G}^*_{Fe(Al)_2O_4} - \overline{G}^*_{Al(Al,Fe)_2O_4}$
	$\Delta\overline{G}^*_{3'3}$	$\overline{G}^*_{Fe^{2+}(Cr)_2O_4} - \overline{G}^*_{Cr(Fe^{2+},Cr)_2O_4}$
	$\Delta\overline{G}^*_{5'5}$	$\overline{G}^*_{Fe^{2+}(Fe^{3+})_2O_4} - \overline{G}^*_{Fe^{3+}(Fe^{2+},Fe^{3+})_2O_4}$
Reciprocal energies	$\Delta\overline{G}^0_{24}$	$\overline{G}^*_{Mg(Mg,Ti)_2O_4} + \overline{G}^*_{Al(Al,Fe)_2O_4} - \overline{G}^*_{Al(Al,Mg)_2O_4} - \overline{G}^*_{Fe(Fe,Ti)_2O_4}$
	$\Delta\overline{G}^0_{25}$	$\overline{G}^*_{Fe^{3+}(Mg,Fe^{3+})_2O_4} + \overline{G}^*_{Al(Al,Fe)_2O_4} - \overline{G}^*_{Al(Al,Mg)_2O_4} - \overline{G}^*_{Fe^{3+}(Fe^{2+},Fe^{3+})_2O_4}$
Exchange and reciprocal ordering energies	$\Delta\overline{G}^0_X$	$\overline{G}^*_{Mg(Fe,Ti)_2O_4} + \overline{G}^*_{Fe(Mg,Ti)_2O_4} - \overline{G}^*_{Mg(Mg,Ti)_2O_4} - \overline{G}^*_{Fe(Fe,Ti)_2O_4}$
	$\Delta\overline{G}^0_{EX}$	$\overline{G}^*_{Mg(Fe,Ti)_2O_4} - \overline{G}^*_{Fe(Mg,Ti)_2O_4}$
Parameter type	Label	Relevant join(s)
Order-disorder regular solution parameters	$W_{1'1}$	$Fe(Al)_2O_4$-$Al(Fe,Al)_2O_4$
	$W_{2'2}$	$Mg(Al)_2O_4$-$Al(Mg,Al)_2O_4$
	$W_{5'5}$	$Fe^{2+}(Fe^{3+})_2O_4$-$Fe^{3+}(Fe^{2+},Fe^{3+})_2O_4$
Regular solution parameters	$^{[4]}W_{FeMg}$	$Fe(Al)_2O_4$-$Mg(Al)_2O_4$
		$Fe(Fe,Ti)_2O_4$-$Mg(Fe,Ti)_2O_4$
		$Fe(Mg,Ti)_2O_4$-$Mg(Mg,Ti)_2O_4$
		$Fe^{2+}(Fe^{3+})_2O_4$-$Mg(Fe^{3+})_2O_4$
		$Fe^{2+}(Cr)_2O_4$-$Mg(Cr)_2O_4$
	$^{[6]}W_{FeMg}$	$Al(Fe,Al)_2O_4$-$Al(Mg,Al)_2O_4$
		$Fe(Fe,Ti)_2O_4$-$Fe(Mg,Ti)_2O_4$
		$Mg(Fe,Ti)_2O_4$-$Mg(Mg,Ti)_2O_4$
		$Fe^{3+}(Fe^{2+},Fe^{3+})_2O_4$-$Fe^{3+}(Mg,Fe^{3+})_2O_4$
	$W_{13'}$	$Al(Fe,Al)_2O_4$-$Fe^{2+}(Cr)_2O_4$
	$W_{1'3'}$	$Fe(Al)_2O_4$-$Fe^{2+}(Cr)_2O_4$
		$Mg(Al)_2O_4$-$Mg(Cr)_2O_4$
	W_{14}	$Al(Fe,Al)_2O_4$-$Fe(Fe,Ti)_2O_4$
	$W_{1'4}$	$Fe(Al)_2O_4$-$Fe(Fe,Ti)_2O_4$
	W_{15}	$Al(Fe,Al)_2O_4$-$Fe^{3+}(Fe^{2+},Fe^{3+})_2O_4$
		$Al(Mg,Al)_2O_4$-$Fe^{3+}(Mg,Fe^{3+})_2O_4$
	$W_{1'5}$	$Fe(Al)_2O_4$-$Fe^{3+}(Fe^{2+},Fe^{3+})_2O_4$
	$W_{15'}$	$Al(Fe,Al)_2O_4$-$Fe^{2+}(Fe^{3+})_2O_4$
	$W_{1'5'}$	$Fe(Al)_2O_4$-$Fe^{2+}(Fe^{3+})_2O_4$
		$Mg(Al)_2O_4$-$Mg(Fe^{3+})_2O_4$
	$W_{23'}$	$Al(Mg,Al)_2O_4$-$Mg(Cr)_2O_4$
	W_{24}	$Al(Mg,Al)_2O_4$-$Mg(Mg,Ti)_2O_4$
	$W_{2'4}$	$Mg(Al)_2O_4$-$Mg(Mg,Ti)_2O_4$
	$W_{2'5}$	$Mg(Al)_2O_4$-$Fe^{3+}(Mg,Fe^{3+})_2O_4$
	$W_{25'}$	$Al(Mg,Al)_2O_4$-$Mg(Fe^{3+})_2O_4$
	$W_{3'4}$	$Fe^{2+}(Cr)_2O_4$-$Fe(Fe,Ti)_2O_4$
	$W_{3'5}$	$Fe^{2+}(Cr)_2O_4$-$Fe^{3+}(Fe^{2+},Fe^{3+})_2O_4$
	$W_{3'5'}$	$Fe^{2+}(Cr)_2O_4$-$Fe^{2+}(Fe^{3+})_2O_4$
	$W_{3'4}$	$Mg(Cr)_2O_4$-$Mg(Mg,Ti)_2O_4$
	W_{45}	$Fe(Fe,Ti)_2O_4$-$Fe^{3+}(Fe^{2+},Fe^{3+})_2O_4$
	$W_{45'}$	$Fe(Fe,Ti)_2O_4$-$Fe^{2+}(Fe^{3+})_2O_4$
	$W_{4'5'}$	$Mg(Mg,Ti)_2O_4$-$Mg(Fe^{3+})_2O_4$

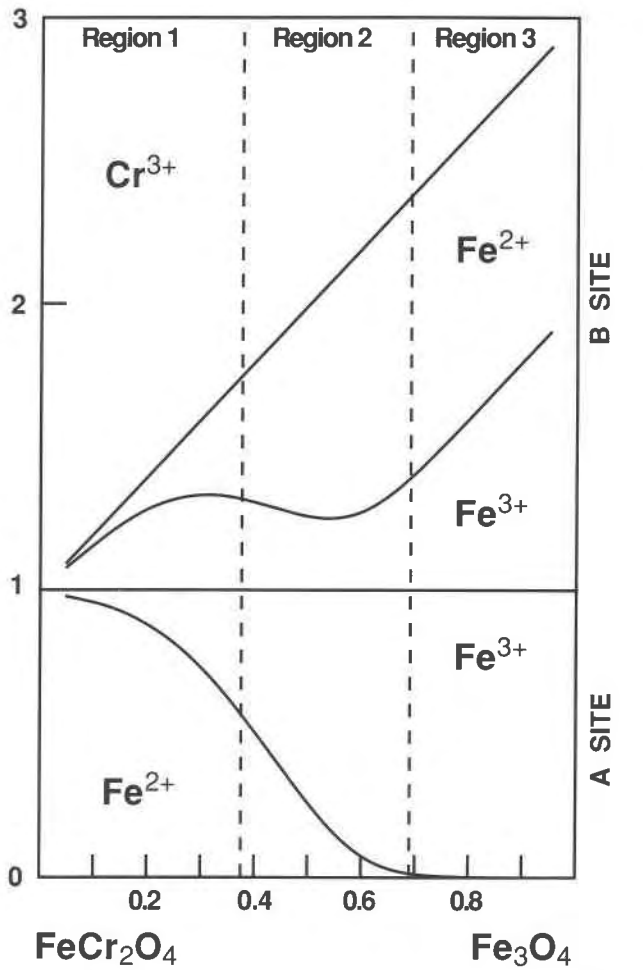

Fig. 1. Site distributions calculated for chromite-magnetite solid solutions at 25 °C compared with approximate boundaries between regions of differing cation ordering schemes inferred from Mössbauer, magnetic, and volume-composition data (Robbins et al., 1971). Regions 1 and 3 are the composition ranges for which $RT \ln ({}^{[4]}X_{Fe^{3+}}\,{}^{[6]}X_{Fe^{2+}})/({}^{[4]}X_{Fe^{2+}}\,{}^{[6]}X_{Fe^{3+}})$ (Eq. 10) is either strongly negative or positive (i.e., regions in which magnetite behaves primarily as a normal and inverse component, respectively).

the high-temperature (600–1000 °C) refinements of Peterson et al. (in preparation) using neutron diffraction require that $MgAl_2O_4$ exhibits a smaller dependence of the degree of Al-Mg order (s_2) on temperature, with $0.64 \leq s_2 \leq 0.66$ at 1000 °C and $0.80 \leq s_2 \leq 0.83$ at 600 °C. Consequently, we have derived appropriate values for $\Delta\overline{H}^*_{2'2}$ (−18.4 kJ) and $W_{2'2}$ (15.1 kJ) and revised the values of other related parameters for $(Fe,Mg)(Al,Fe^{3+})_2O_4$-$(Fe,Mg)_2TiO_4$ (Table 4) to achieve internal consistency with the remaining constraints enumerated by Sack and Ghiorso (1991).

Calibration of the thermodynamic parameters pertinent to chromian spinels ($W_{13'}$, $W_{1'3'}$, $W_{23'}$, $W_{3'4}$, $W_{3'4}$, $W_{3'5}$, $W_{3'5'}$) logically proceeds with $FeCr_2O_4$-Fe_3O_4, because numerous studies bear on their thermodynamic properties. Of particular interest are constraints on site distributions at low temperatures (e.g., Robbins et al., 1971) and the determinations of the activities of Fe_3O_4 at 1400 °C (Petric and Jacob, 1982a) and 1223 °C (Katsura et al., 1975). The low-temperature constraints on site occupancies in $FeCr_2O_4$-Fe_3O_4 spinels indicate that Fe^{3+} undergoes a progressive change in site preference with composition. In Cr-rich compositions Fe^{3+} is primarily octahedral (i.e., Fe_3O_4 behaves as a normal spinel component), despite the fact that Fe_3O_4 has a Fe^{2+}-Fe^{3+} distribution that is more inverse than random, even at high temperatures (e.g., Sack and Ghiorso, 1991). Assuming

TABLE 3. Definition of $\bar{G}$ in terms of the preferred thermodynamic parameters

$$\begin{aligned}
\bar{G}^* = {} & \bar{G}_1^* + [\tfrac{1}{2}({}^{[6]}W_{\mathrm{FeMg}} + W_{2\underline{4}} - W_{1\underline{4}} + \Delta\bar{G}^0_{2\underline{4}}) + \tfrac{1}{4}(\Delta\bar{G}^0_X + \Delta\bar{G}^0_{EX}) + \bar{G}_2^* - \bar{G}_1^*]X_2 + (W_{1\underline{3}'} + \Delta\bar{G}^*_{3\underline{3}} + \bar{G}_3^* - \bar{G}_1^*)X_3 + (W_{1\underline{4}} + \bar{G}_4^* - \bar{G}_1^*)X_4 \\
& + (W_{1\underline{5}} + \bar{G}_5^* - \bar{G}_1^*)X_5 + [\tfrac{1}{2}(W_{2\underline{4}} - W_{1\underline{4}} - {}^{[6]}W_{\mathrm{FeMg}} + \Delta\bar{G}^0_{2\underline{4}}) + \tfrac{1}{4}(\Delta\bar{G}^0_X + \Delta\bar{G}^0_{EX})]s_1 + (W_{1'1} + \Delta\bar{G}^*_{1'1})s_2 + (W_{1\underline{5}'} - W_{1\underline{5}} + \Delta\bar{G}^*_{5\underline{5}})s_4 \\
& - \tfrac{1}{4}({}^{[4]}W_{\mathrm{FeMg}} + {}^{[6]}W_{\mathrm{FeMg}} + \Delta\bar{G}^0_X)X_2^2 - W_{1\underline{3}'}X_3^2 - W_{1\underline{4}}X_4^2 - W_{1\underline{5}}X_5^2 - \tfrac{1}{4}({}^{[4]}W_{\mathrm{FeMg}} + {}^{[6]}W_{\mathrm{FeMg}} - \Delta\bar{G}^0_X)s_1^2 - W_{1'1}s_2^2 - W_{5\underline{5}'}s_4^2 \\
& + [\tfrac{1}{2}({}^{[4]}W_{\mathrm{FeMg}} - {}^{[6]}W_{\mathrm{FeMg}} + W_{1\underline{3}'} - W_{2\underline{3}'} - \Delta\bar{G}^0_{EX}) + W_{3'\underline{4}} - W_{3'4} + \Delta\bar{G}^0_{2\underline{4}}]X_2X_3 + [\tfrac{1}{2}({}^{[4]}W_{\mathrm{FeMg}} + W_{1\underline{4}} - W_{2\underline{4}} + \Delta\bar{G}^0_{2\underline{4}}) + \tfrac{1}{4}(\Delta\bar{G}^0_X - \Delta\bar{G}^0_{EX})]X_2X_4 \\
& + [\tfrac{1}{2}(W_{2\underline{5}'} - W_{1\underline{5}} + W_{1'1} - W_{2'2}) + \Delta\bar{G}^0_{2\underline{5}}]X_2X_5 + \tfrac{1}{2}({}^{[6]}W_{\mathrm{FeMg}} - {}^{[4]}W_{\mathrm{FeMg}})X_2s_1 + [\tfrac{1}{2}({}^{[4]}W_{\mathrm{FeMg}} - {}^{[6]}W_{\mathrm{FeMg}} + W_{1'1} - W_{2'2} - \Delta\bar{G}^0_{EX}) \\
& + W_{2'\underline{4}} - W_{1'4} + \Delta\bar{G}^0_{2\underline{4}}]X_2s_2 + [\tfrac{1}{2}({}^{[4]}W_{\mathrm{FeMg}} - {}^{[6]}W_{\mathrm{FeMg}} + W_{1\underline{5}} - W_{2\underline{5}'} + W_{1\underline{5}'} - W_{2\underline{5}'} + W_{2'2} - W_{1'1} - \Delta\bar{G}^0_{EX}) + W_{4\underline{5}'} - W_{4\underline{5}'} + \bar{G}^0_{2\underline{4}} - \Delta\bar{G}^0_{2\underline{5}}]X_2s_4 \\
& + (W_{3'4} - W_{1\underline{3}'} - W_{1\underline{4}})X_3X_4 + (W_{3'\underline{5}} - W_{1\underline{3}'} - W_{1\underline{5}})X_3X_5 + \tfrac{1}{2}({}^{[4]}W_{\mathrm{FeMg}} + {}^{[6]}W_{\mathrm{FeMg}} + W_{1\underline{3}'} - W_{2\underline{3}'} - \Delta\bar{G}^0_X)X_3s_1 + (W_{1'\underline{3}'} - W_{1\underline{3}'} - W_{1'1})X_3s_2 \\
& + (W_{3'\underline{5}'} - W_{3'\underline{5}} + W_{1\underline{5}} - W_{1\underline{5}'})X_3s_4 + (W_{4\underline{5}} - W_{1\underline{4}} - W_{1\underline{5}})X_4X_5 + [\tfrac{1}{2}({}^{[4]}W_{\mathrm{FeMg}} + W_{1\underline{4}} - W_{2\underline{4}} - \Delta\bar{G}^0_{2\underline{4}}) + \tfrac{1}{4}(\Delta\bar{G}^0_{EX} - \Delta\bar{G}^0_X)]X_4s_1 \\
& + (W_{1'4} - W_{1\underline{4}} - W_{1'1})X_4s_2 + (W_{4\underline{5}'} - W_{4\underline{5}} + W_{1\underline{5}} - W_{1\underline{5}'})X_4s_4 + \tfrac{1}{2}(W_{2\underline{5}'} - W_{1\underline{5}} + W_{1'1} - W_{2'2})X_5s_1 + (W_{1\underline{5}} - W_{1\underline{5}} - W_{1'1})X_5s_2 \\
& + (W_{1\underline{5}} - W_{1\underline{5}'} + W_{5\underline{5}'})X_5s_4 + \tfrac{1}{2}({}^{[4]}W_{\mathrm{FeMg}} + {}^{[6]}W_{\mathrm{FeMg}} + W_{1'1} - W_{2'2} - \Delta\bar{G}^0_X)s_1s_2 \\
& + \tfrac{1}{2}({}^{[4]}W_{\mathrm{FeMg}} + {}^{[6]}W_{\mathrm{FeMg}} + W_{1\underline{5}'} - W_{2\underline{5}'} + W_{1\underline{5}} - W_{2\underline{5}} + W_{2'2} - W_{1'1} - \Delta\bar{G}^0_X)s_1s_4 + (W_{1\underline{5}} - W_{1\underline{5}'} + W_{1'\underline{5}'} - W_{1'\underline{5}})s_2s_4 \\
\bar{S}^{IC} = {} & -R\left[\frac{X_2 + s_1}{2}\ln\left(\frac{X_2 + s_1}{2}\right) + \left(X_3 + X_4 + s_2 + s_4 - \frac{X_2 + s_1}{2}\right)\ln\left(X_3 + X_4 + s_2 + s_4 - \frac{X_2 + s_1}{2}\right)\right. \\
& + (X_5 - s_4)\ln(X_5 - s_4) + (1 - X_3 - X_4 - X_5 - s_2)\ln(1 - X_3 - X_4 - X_5 - s_2) + 2X_3\ln X_3 + \frac{X_2 - s_1}{2}\ln\left(\frac{X_2 - s_1}{4}\right) \\
& + \left(1 - X_3 - s_2 - s_4 - \frac{X_2 - s_1}{2}\right)\ln\left(\frac{1 - X_3 - s_2 - s_4}{2} - \frac{X_2 - s_1}{4}\right) + (X_5 + s_4)\ln\left(\frac{X_5 + s_4}{2}\right) \\
& \left. + (1 - X_3 - X_4 - X_5 + s_2)\ln\left(\frac{1 - X_3 - X_4 - X_5 + s_2}{2}\right) + X_4\ln\frac{X_4}{2}\right] \\
\bar{G} = {} & \bar{G}^* - T\bar{S}^{IC}
\end{aligned}$$

that $W_{5'5}$ is negligible and $\Delta\overline{H}^*_{5'5} \sim 30$ kJ/gfw (Sack and Ghiorso, 1991), $W_{3'5}$ must be about 40 kJ/gfw larger than $W_{3'5'}$ to generate values of $RT\ \ln({}^{[4]}X_{Fe^{3+}}{}^{[6]}X_{Fe^{2+}})/({}^{[4]}X_{Fe^{2+}}{}^{[6]}X_{Fe^{3+}})$ from the condition of homogeneous equilibrium $(\partial\bar{G}/\partial s_4) = 0$,

$$RT\ln\left(\frac{{}^{[4]}X_{Fe^{3+}}\,{}^{[6]}X_{Fe^{2+}}}{{}^{[4]}X_{Fe^{2+}}\,{}^{[6]}X_{Fe^{3+}}}\right) = \Delta\bar{G}^*_{5'5} + W_{5'5}(1 - 2s_4) + (W_{3'5'} - W_{5'5} - W_{3'5})(1 - X_5) \qquad (10)$$

that are consistent with the observation that Fe^{3+} is primarily octahedral in Cr-rich compositions. Both the site distribution (Fig. 1) and activity-composition constraints (Fig. 2) are satisfied if $W_{3'5}$ is about 42 kJ/gfw and $W_{3'5'}$ is negligible. The inference that $W_{3'5'}$ is negligible agrees with size considerations (i.e., the octahedral radii of Cr^{3+} and Fe^{3+} are similar) and is required to duplicate the functional form of the activity-composition constraints.

Several types of data bear on the calibration of the parameters $W_{3'4}$, $W_{3'4}$, $W_{1\underline{3}'}$, $W_{2\underline{3}'}$, and $W_{1'\underline{3}'}$. They include (1) approximate bound on the extents to which miscibility gaps in $FeAl_2O_4$-Fe_2TiO_4 and $MgAl_2O_4$-Mg_2TiO_4 protrude into ternary subsystems containing $FeCr_2O_4$ or $MgCr_2O_4$ over the temperature range 1000–1300 °C (Muan et al., 1972), (2) Al-Cr partitioning for $(Al,Cr)_2O_3$ solid solutions coexisting with $Fe(Al,Cr)_2O_4$ and $Mg(Al,Cr)_2O_4$ (Petric and Jacob, 1982b; Oka et al., 1984) and $Na(Al,Cr)_2Si_2O_6$ coexisting with $Mg(Al,Cr)_2O_4$ (Carroll Webb and Wood, 1986), and (3) both experimental and petrological constraints on Fe-Mg partitioning between olivine and $(Fe,Mg)(Al,Cr,Fe^{3+})_2O_4$-$(Fe,Mg)_2TiO_4$ (Sack, 1982; Engi, 1983; Jamieson and Roeder, 1984; Lehmann and Roux, 1986; Hill and Sack, 1987; Allan et al., 1987, 1988). A value for $W_{3'4}$ of about 41.84 kJ/gfw is in reasonable accord with the approximate constraints of Muan et al. (1972) for $FeAl_2O_4$-Fe_2TiO_4-$FeCr_2O_4$ at 1000 °C (Fig. 3a). Such a value is near the upper bound permitted by the inference that Fe_2TiO_4-$FeCr_2O_4$ exhibit complete

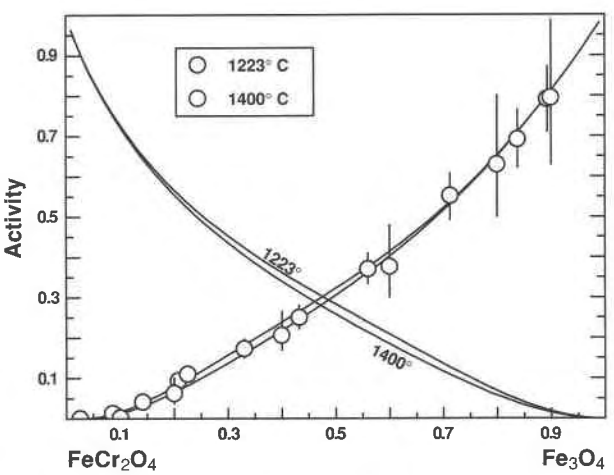

Fig. 2 Calculated activity-composition relations for Fe-Cr_2O_4-Fe_3O_4 compared with experimental determinations of Fe_3O_4 activity. Vertical lines indicate the 1σ error associated with the Fe_3O_4 activity determinations of Katsura et al. (1975; 1223 °C) and Petric and Jacob (1982a; 1400 °C).

TABLE 4. Preferred values of model parameters (kJ)

Parameter	Value (kJ)	
		$FeAl_2O_4$
$\Delta\overline{H}_{1'1}$	−36.401	
$\Delta\overline{S}_{1'1}$	0.000*	
$W_{1'1}$	18.828	
		$MgAl_2O_4$
$W_{2'2}$	15.062	
		$FeCr_2O_4$
$\Delta\overline{H}_{3'3}$	$-\infty$	Assumed negative enough to stabilize the normal structure at all temperatures
$\Delta\overline{S}_{3'3}$	0.000*	
		Fe_3O_4
$\Delta\overline{H}_{5'5}$	26.150	
$\Delta\overline{S}_{5'5}$	0.000*	
$W_{5'5}$	0.000	
		Reciprocal terms
$\Delta\overline{H}^0_{24}$	27.405	Reaction: ½ Fe_2TiO_4 + $Al(Mg,Al)_2O_4$ = ½ Mg_2TiO_4 + $Al(Fe,Al)_2O_4$
$\Delta\overline{S}^0_{24}$	0.000*	
$\Delta\overline{H}^0_{25}$	33.681	Reaction: $Fe^{3+}(Fe^{2+},Fe^{3+})_2O_4$ + $Al(Mg,Al)_2O_4$ = $Fe(Mg,Fe)_2O_4$ + $Al(Fe,Al)_2O_4$
$\Delta\overline{S}^0_{25}$	0.000*	
$\Delta\overline{H}^0_{EX}$	−15.062	Reaction: $Fe(Mg,Ti)_2O_4$ = $Mg(Fe,Ti)_2O_4$
$\Delta\overline{S}^0_{EX}$	0.000*	
$\Delta\overline{H}^0_{X}$	10.042	Reaction: Fe_2TiO_4 + Mg_2TiO_4 = $Fe(Mg,Ti)_2O_4$ + $Mg(Fe,Ti)_2O_4$
$\Delta\overline{S}^0_{X}$	0.000*	
		Standard state parameters
$\Delta\overline{H}^0_{21}$	−369.866	defined as $\overline{H}^*_2 - \overline{H}^*_1$
$\Delta\overline{S}^0_{21}$	−0.04100	defined as $\overline{S}^*_2 - \overline{S}^*_1$
		Interaction parameters
$^{[6]}W_{FeMg}$	8.368	definition for W_{12}
W_{13}	47.279	
W_{14}	87.027	
W_{15}	41.840	
$W_{15'}$	48.953	
$^{[4]}W_{FeMg}$	8.368	definition for $W_{1'2'}$
$W_{1'3'}$	24.686	
$W_{1'4}$	51.882	
$W_{1'5}$	60.250	
$W_{1'5'}$	29.288	
$W_{23'}$	40.585	
W_{24}	52.718	
$W_{25'}$	64.015	
$W_{2'4}$	45.606	
$W_{2'5}$	60.250	
$W_{3'4}$	41.840	
$W_{3'4}$	43.514	
$W_{3'5}$	41.840	
$W_{3'5'}$	0.000	
W_{45}	25.104	
$W_{45'}$	8.368	
$W_{46'}$	7.531	

Note: Brackets denote octahedral sites.
* Required for temperature independent W parameters.

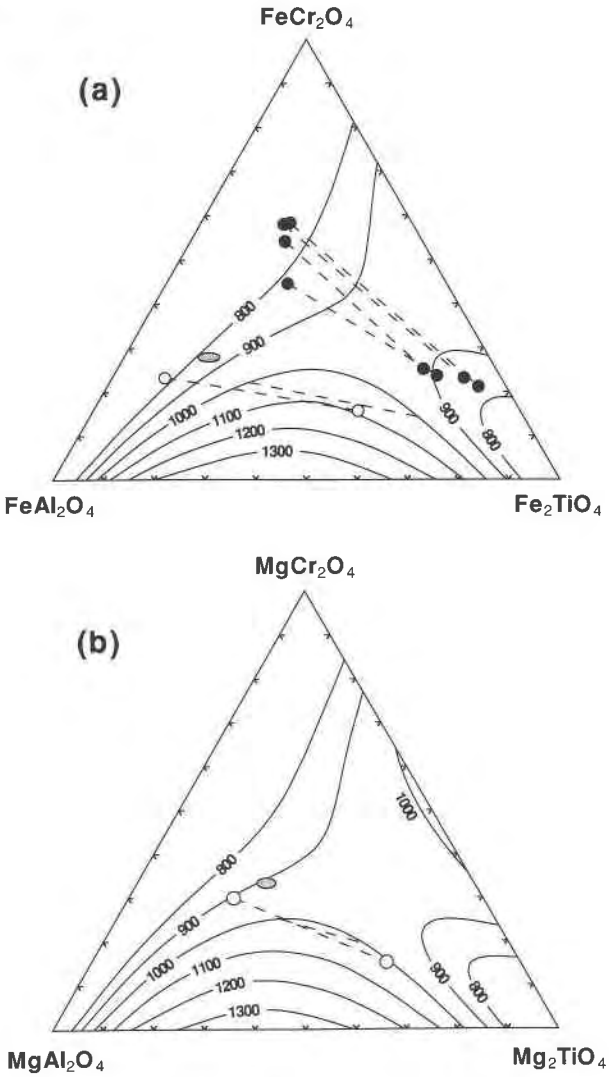

Fig. 3. Calculated miscibility gaps for **a** $FeAl_2O_4$-$FeCr_2O_4$-Fe_2TiO_4 and **b** $MgAl_2O_4$-$MgCr_2O_4$-Mg_2TiO_4 compared with experimental constraints and composition data for coexisting Cr- and Ti-rich spinels in lunar basalts. (**a**) The solid curves represent miscibility gaps for $FeAl_2O_4$-$FeCr_2O_4$-Fe_2TiO_4 calculated for 800, 900, 1000, 1100, 1200, and 1300 °C. The shaded ellipse and open circles connected by a dashed line indicate the approximate constraints on the extent of ternary miscibility and the sense of a tie line for coexisting ternary spinels. These results were estimated from X-ray determinative curves and synthesis experiments by Muan et al. (1972). The dashed line connecting points on the 1000 °C miscibility gap is a comparable calculated tie line. The solid circles connected by dashed lines indicate the composition data reported by Agrell et al. (1970), Champness et al. (1971), Haggerty and Meyer (1970), and Taylor et al. (1971) for coexisting Cr- and Ti-rich spinels in lunar basaltic rocks. (**b**) The solid curves represent miscibility gaps for $MgAl_2O_4$-$MgCr_2O_4$-Mg_2TiO_4 calculated for 800, 900, 1000, 1100, 1200, and 1300 °C. Symbols are analogous to those in **a**.

miscibility down to temperatures of at least 1000 °C (e.g., Evans and Moore, 1968; Muan et al., 1972). Smaller values of $W_{3'4}$ are unlikely because the size of this parameter is the chief factor determining the extent of ternary solid solution in light of plausible values for the parameters $W_{13'}$ and $W_{1'3'}$ permitted by the other data. However, the approximate constraints of Muan et al. (1972) for $MgAl_2O_4$-Mg_2TiO_4-$MgCr_2O_4$ (Fig. 3b) do not place similarly tight bounds on the analogous parameter $W_{3'4}$. Because

$MgAl_2O_4$ is significantly more disordered than $FeAl_2O_4$ (e.g., Sack and Ghiorso, 1991), the extent of ternary solid solution calculated for $MgAl_2O_4$-Mg_2TiO_4-$MgCr_2O_4$ is equally sensitive to the size of the parameter $W_{23'}$. We may safely assume, however, that upper bounds on $W_{3'4}$ are similar to those on $W_{3'4}$ because high-temperature miscibility gaps are also not evident in Mg_2TiO_4-$MgCr_2O_4$ (cf. Muan et al., 1972).

Constraints on the parameters $W_{13'}$, $W_{23'}$, and $W_{1'3'}$ may be readily derived from Al-Cr partitioning data for $(Al,Cr)_2O_3$ solid solutions coexisting with $Fe(Al,Cr)_2O_4$ and $Mg(Al,Cr)_2O_4$ (Petric and Jacob, 1982b; Oka et al., 1984). As we will demonstrate, these constraints also bear on the size of the parameter sum ($W_{3'4} + W_{13'} - W_{3'4} - W_{23'}$) appearing in the expression for $\Delta\bar{G}_{23}^{0(N)}$ (Eq. 9), because we have assumed that the vibrational Gibbs energy may be satisfactorily described by a Taylor expansion of only second degree in composition and ordering variables (i.e., no ternary terms are required). Because this parameter sum is also constrained by Fe-Mg partitioning between olivine and chromian spinels, a consistent value for it must be obtained from the analysis of both Al-Cr and Fe-Mg partitioning. Analysis of the data for $Fe(Al,Cr)_2O_4$ is the most straightforward because activity-composition relations for $(Al,Cr)_2O_3$ solid solutions are well known (Jacob, 1978; Chatterjee et al., 1982) and $FeAl_2O_4$ is substantially normal at the temperature (1100 °C) at which Al-Cr partitioning between $(Al,Cr)_2O_3$ and $Fe(Al,Cr)_2O_4$ has been determined by Petric and Jacob (1982b). Accordingly, the term $(W_{1'1} - W_{13'})(1 - X_3 - s_2)$ is small in the expression for the $(Cr,Al)_{-1}$ exchange potential. For $Fe(Al,Cr)_2O_4$ referenced to normal cation ordering states, this expression is given by

$$\begin{aligned} &\tfrac{1}{2}(\partial\bar{G}/\partial X_3) + \tfrac{1}{2}(\partial\bar{G}/\partial s_2) \\ &= \tfrac{1}{2}(\bar{G}^*_{3'} - \bar{G}^*_{1'}) + RT\ln\left[\frac{{}^{[6]}X_{Cr^{3+}}}{{}^{[6]}X_{Al^{3+}}}\right] \\ &\quad - \tfrac{1}{2}(W_{1'1} - W_{13'})(1 - X_3 - s_2) \\ &\quad + \tfrac{1}{2}W_{1'3'}(s_2 - X_3). \end{aligned} \tag{11}$$

Therefore, a fairly well-constrained estimate for the parameter $W_{1'3'}$ may be obtained by evaluating the slope defined by the exchange data of Petric and Jacob (1982b). We proceed by utilizing the condition of Cr-Al exchange equilibrium between $(Al,Cr)_2O_3$ and $Fe(Al,Cr)_2O_4$

$$\mu^{Ox}_{Cr(Al)_{-1}} = {}^{(N)}\mu^{Fe\text{-}Sp}_{Cr(Al)_{-1}} \tag{12}$$

and define a thermodynamic quantity analogous to the logarithm of the distribution coefficient,

$$\begin{aligned} \bar{Q}^{*Fe\text{-}Sp}_{Cr(Al)_{-1}} &\equiv RT\ln\left(\frac{a^{Ox}_{Cr_2O_3}}{a^{Ox}_{Al_2O_3}}\right) - RT\ln\left(\frac{{}^{[6]}X_{Cr^{3+}}}{{}^{[6]}X_{Al^{3+}}}\right) \\ &\quad + \tfrac{1}{2}(W_{1'1} - W_{13'})(1 - X_3 - s_2) \\ &= \Delta\bar{G}^{0\ Fe\text{-}Sp}_{Cr(Al)_{-1}} + \tfrac{1}{2}W_{1'3'}(s_2 - X_3) \end{aligned} \tag{13}$$

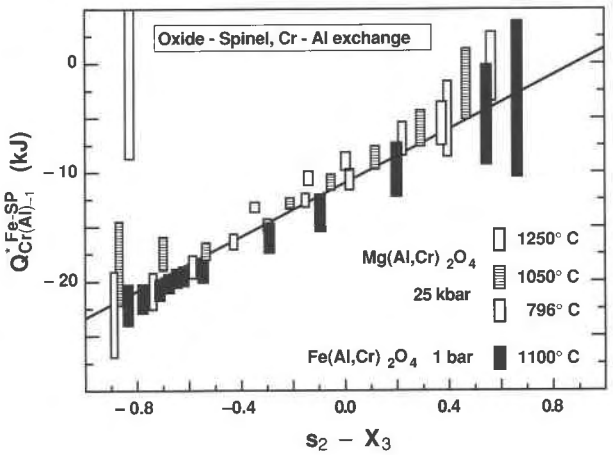

Fig. 4. Calibration for $\bar{Q}^{*Fe\text{-}Sp}_{Cr(Al)_{-1}}$ (Eqs. 13 and 17) compared with experimental constraints. Solid bars indicate extreme values of $\bar{Q}^{*Fe\text{-}Sp}_{Cr(Al)_{-1}}$ and $(s_2 - X_3)$ that are consistent with the partitioning data of Petric and Jacob (1982b) at 1100 °C and 1 atm for Al-Cr exchange between $(Al,Cr)_2O_3$ solid solutions and $Fe(Al,Cr)_2O_4$. Shaded and ruled bars represent extreme values of $\bar{Q}^{*Fe\text{-}Sp}_{Cr(Al)_{-1}}$ and $(s_2 - X_3)$ calculated from the data of Oka et al. (1984) at 1250 and 1050 °C (25 kbar) for partitioning of Al and Cr between $(Al,Cr)_2O_3$ solid solutions and $Mg(Al,Cr)_2O_4$. The widths and lengths of bars are consistent with an assumed uncertainty of 0.010 in the ratios of Al/(Al + Cr) in the exchanging phases and do not incorporate errors arising from uncertainties in activity-composition relations of $(Al,Cr)_2O_3$ solid solutions or volume-composition relations in $(Al,Cr)_2O_3$ or $Mg(Al,Cr)_2O_4$ solid solutions (see text). The diagonal line denotes the calibration of $\bar{Q}^{*Fe\text{-}Sp}_{Cr(Al)_{-1}}$ based on the values of the thermodynamic parameters given in Table 4. This line has a slope corresponding to one-half of the value of the parameter $W_{1'3'}$. The data of Oka et al. (1984) at 796 °C (open bars) are shown for comparison only.

where $\Delta\bar{G}^{0\ Fe\text{-}Sp}_{Cr(Al)_{-1}}$ is the standard state Gibbs free energy change of the reaction

$$\tfrac{1}{2}Cr_2O_3 + \tfrac{1}{2}Fe(Al)_2O_4 = \tfrac{1}{2}Al_2O_3 + \tfrac{1}{2}Fe(Cr)_2O_4.$$

Expressions for $a^{Ox}_{Cr_2O_3}$ and $a^{Ox}_{Al_2O_3}$ are derived from the calibration for thermodynamic properties of $(Al,Cr)_2O_3$ of Chatterjee et al. (1982), and the ordering variable s_2 is given by solution of the condition of homogeneous equilibrium for $FeAl_2O_4$-$FeCr_2O_4$:

$$\begin{aligned} 0 &= (\partial\bar{G}/\partial s_2) \\ &= RT\ln\left(\frac{{}^{[4]}X_{Fe^{2+}}\,{}^{[6]}X_{Al^{3+}}}{{}^{[4]}X_{Al^{3+}}\,{}^{[6]}X_{Fe^{2+}}}\right) + \Delta\bar{G}^*_{1'1} + W_{1'1}(1 - 2s_2) \\ &\quad + (W_{1'3'} - W_{1'1} - W_{13'})X_3. \end{aligned} \tag{14}$$

A value for $W_{1'3'}$ of about 25 kJ/gfw is required (Fig. 4) by the data of Petric and Jacob (1982b).

We may also derive a comparable set of equations to describe $Cr(Al)_{-1}$ partitioning at 25 kbar between $(Al,Cr)_2O_3$ and $Mg(Al,Cr)_2O_4$ (Oka et al., 1984), providing we make the approximations that (1) s_2 does not depend

on pressure and that (2) the effects of temperature and pressure on molar volumes cancel across the $Cr(Al)_{-1}$ exchange. With these approximations, the condition of $Cr(Al)_{-1}$ exchange equilibrium may be written

$$\begin{aligned} 0 = &-RT\ln\left(\frac{a^{Ox}_{Cr_2O_3}}{a^{Ox}_{Al_2O_3}}\right)_{1,T} - P\bar{V}^{ex\ Ox}_{Cr(Al)_{-1}} \\ &+ RT\ln\left(\frac{[6]X_{Cr^{3+}}}{[6]X_{Al^{3+}}}\right) + P\bar{V}^{ex\ Mg\text{-}Sp}_{Cr(Al)_{-1}} \\ &- \tfrac{1}{2}(W_{2'2} - W_{23'})(1 - X_3 - s_2) + \tfrac{1}{2}W_{1'3'}(s_2 - X_3) \\ &+ (\Delta\bar{G}^{0\ Mg\text{-}Sp}_{Cr(Al)_{-1}})_{1,T} + P\Delta\bar{V}^{0\ Mg\text{-}Sp}_{Cr(Al)_{-1}}. \end{aligned} \quad (15)$$

In this expression $\Delta\bar{G}^{0\ Mg\text{-}Sp}_{Cr(Al)_{-1}}$ is the standard state free energy change of the reaction $\frac{1}{2}Cr_2O_3 + \frac{1}{2}Mg(Al)_2O_4 = \frac{1}{2}Al_2O_3 + \frac{1}{2}Mg(Cr)_2O_4$, and $\Delta\bar{V}^{0\ Mg\text{-}Sp}_{Cr(Al)_{-1}}$ is equal to 0.0179 kJ/gfw (Oka et al., 1984). Expressions for $\bar{V}^{ex\ Mg\text{-}Sp}_{Cr(Al)_{-1}}$ and $\bar{V}^{ex\ Ox}_{Cr(Al)_{-1}}$ may be derived from those given for the excess volumes of $Mg(Al,Cr)_2O_4$ and $(Al,Cr)_2O_3$ by Oka et al. (1984) and Chatterjee et al. (1982), respectively. The ordering variable s_2 is provided by solution of the condition of homogeneous equilibrium for $MgAl_2O_4$-$MgCr_2O_4$,

$$\begin{aligned} 0 &= (\partial\bar{G}/\partial s_2) \\ &= RT\ln\left(\frac{[4]X_{Mg^{2+}}\,[6]X_{Al^{3+}}}{[4]X_{Al^{3+}}\,[6]X_{Mg^{2+}}}\right) + \Delta\bar{G}^{*}_{2'2} + W_{2'2}(1 - 2s_2) \\ &\quad + (W_{1'3'} - W_{2'2} - W_{23'})X_3 \end{aligned} \quad (16)$$

where $\Delta\bar{G}^{*}_{2'2}$ is a dependent parameter (see Eq. 8 and Table 6 of Sack and Ghiorso, 1991). Taking into account the relation between $(\Delta\bar{G}^{0\ Mg\text{-}Sp}_{Cr(Al)_{-1}})_{1,T}$ and $(\Delta\bar{G}^{0\ Fe\text{-}Sp}_{Cr(Al)_{-1}})_{1,T}$ given by Equation 9, $\Delta\bar{G}^{0\ Mg\text{-}Sp}_{Cr(Al)_{-1}} = \Delta\bar{G}^{0\ Fe\text{-}Sp}_{Cr(Al)_{-1}} + \Delta\bar{G}^{0(N)}_{23}$, we may rewrite Equation 15 into a form for which the data obtained at 25 kbar bearing on the $Al(Cr)_{-1}$ exchange reaction between $(Al,Cr)_2O_3$ and $Mg(Al,Cr)_2O_4$ (Oka et al., 1984) may be analyzed in conjunction with the data obtained at 1 bar of Petric and Jacob (1982b). This manipulation yields an expression equivalent to Equation 13:

$$\begin{aligned} \bar{Q}^{*\ Fe\text{-}Sp}_{Cr(Al)_{-1}} = &RT\ln\left(\frac{a^{Ox}_{Cr_2O_3}}{a^{Ox}_{Al_2O_3}}\right)_{1,T} + P\bar{V}^{ex\ Ox}_{Cr(Al)_{-1}} \\ &- RT\ln\left(\frac{[6]X_{Cr^{3+}}}{[6]X_{Al^{3+}}}\right) - P\bar{V}^{ex\ Mg-Sp}_{Cr(Al)_{-1}} \\ &+ \tfrac{1}{2}(W_{2'2} - W_{23'})(1 - X_3 - s_2) \\ &- P\Delta\bar{V}^{0\ Mg\text{-}Sp}_{Cr(Al)_{-1}} - \Delta\bar{G}^{0(N)}_{23} \\ = &\Delta\bar{G}^{0\ Fe\text{-}Sp}_{Cr(Al)_{-1}} + \tfrac{1}{2}W_{1'3'}(s_2 - X_3). \end{aligned} \quad (17)$$

Several bounds on $W_{23'}$ and $\Delta\bar{G}^{0(N)}_{23}$ (i.e., the parameter sum $W_{3'4} + W_{13'} - W_{3'4} - W_{23'}$) are readily obtained when the data obtained at 1050 and 1250 °C by Oka et al. (1984) and Petric and Jacob (1982b) are analyzed simultaneously using Equations 13 and 17. We find that the data of Oka et al. (1984) require $W_{23'}$ to be greater than about 40 kJ/gfw to achieve values for the parameter $W_{1'3'}$ comparable with those derived from analysis of the data of Petric and Jacob (1982b). Substantially larger values of $W_{23'}$ are unlikely because they result in calculated miscibility gaps for $MgAl_2O_4$-Mg_2TiO_4-$MgCr_2O_4$ that are much less extensive than those suggested by the experimental constraints of Muan et al. (1972). Values of the parameter sum $(W_{3'4} + W_{13'} - W_{3'4} - W_{23'})$ in the range 8.5–17 kJ/gfw are required for the data of Oka et al. (1984) at 1050 and 1250 °C and the data of Petric and Jacob (1982b) at 1100 °C to be in reasonable accord. Finally, the parameter values derived for $Mg(Al,Cr)_2O_4$ should satisfy the minimum bound on the degree of nonideality of this solid solution determined by Carroll Webb and Wood (1986). From reversed brackets on Al-Cr partitioning between $Na(Al,Cr)Si_2O_6$ and $Mg(Al,Cr)_2O_4$ at 1000 and 1100 °C and 25 kbar, they demonstrate that the maximum nonideality associated with the $Mg(Al,Cr)_2O_4$ solid solution is 5.65 ± 1.05 kJ/gfw, if it is assumed that the $Na(Al,Cr)Si_2O_6$ solution is ideal. The calibration we obtain subsequently results in the comparable value of 6.10 kJ/gfw.

Further constraints on the value of the parameter sum $(W_{3'4} + W_{13'} - W_{3'4} - W_{23'})$ may be derived by considering Fe-Mg partitioning between olivine and Cr-bearing spinels (Sack, 1982; Engi, 1983; Murck and Campbell, 1986; Allan et al., 1987, 1988; Gee and Sack, 1988). Sack and Ghiorso (1991) have developed a calibration of such a relation for olivine coexisting with (Fe,Mg)-$(Al,Fe^{3+})_2O_4$-$(Fe,Mg)_2TiO_4$ over the temperature range 650–1400 °C. To utilize their updated results in our calibration, it is necessary to define the condition of Fe-Mg exchange equilibrium between olivine and (Fe,Mg)-$(Al,Cr,Fe^{3+})_2O_4$-$(Fe,Mg)_2TiO_4$. This condition is given by

$$\mu^{Ol}_{Mg(Fe)_{-1}} = \mu^{Sp}_{Mg(Fe)_{-1}}. \quad (18)$$

The left hand side of Equation 18 may be written

$$\begin{aligned} \mu^{OL}_{Mg(Fe)_{-1}} = &\tfrac{1}{2}(\bar{G}^{0}_{Mg_2SiO_4} - \bar{G}^{0}_{Fe_2SiO_4}) + RT\ln(X^{Ol}_{Mg_2SiO_4}/X^{Ol}_{Fe_2SiO_4}) \\ &+ (\Delta H^{0\ Ol}_{X} + 2\,W^{Ol}_{M})(1 - 2\,X^{Ol}_{Mg_2SiO_4}) \end{aligned} \quad (19)$$

where the standard state Gibbs energies of Mg_2SiO_4 and Fe_2SiO_4 are taken from the data of Berman (1988) and the value of $(\Delta H^{0\ Ol}_{X} + 2\,W^{Ol}_{M})$ is from Sack and Ghiorso (1989). We may expand the right hand side of Equation 18 for spinels in the normal cation ordering state

$$\begin{aligned} \mu^{Sp}_{Mg(Fe)_{-1}} &= {}^{(N)}\mu^{Sp}_{Mg(Fe)_{-1}} \\ &= \mu^{Sp}_{Mg(Al)_2O_4} - \mu^{Sp}_{Fe(Al)_2O_4} = (\partial\bar{G}/\partial X_2) + (\partial\bar{G}/\partial s_1) \end{aligned} \quad (20)$$

and utilize Equation 20 to rewrite Equation 18 in zero intercept form for the ordinate variable X_3, which multiplies the parameter sum $(W_{3'4} + W_{13'} - W_{3'4} - W_{23'})$. These manipulations allow us to define a general thermodynamic equivalent to the traditional ln K_d for equilibrium exchange of Mg and Fe between olivine and spinel:

$$\begin{aligned}\bar{Q}^*_{\text{Al-Cr}} \equiv\ & \mu^{\text{Ol}}_{\text{Mg(Fe)}_{-1}} - \Delta\bar{H}^0_{21} + T\Delta\bar{S}^0_{21} + RT\ln\left(\frac{{}^{[4]}X_{\text{Fe}^{2+}}}{{}^{[4]}X_{\text{Mg}^{2+}}}\right) \\ & + (W_{14} - \Delta\bar{H}^0_{24} - W_{2\underline{4}} - \tfrac{1}{2}\Delta\bar{H}^0_{X'} - \tfrac{1}{2}\Delta\bar{H}^0_{EX}) \\ & + ({}^{[4]}W_{\text{FeMg}} - \tfrac{1}{2}\Delta\bar{H}^0_X)s_1 \\ & - ({}^{[4]}W_{\text{FeMg}} - W_{2'2} + W_{1'1} + W_{2'\underline{4}} - W_{1'4} \\ & \quad - \tfrac{1}{2}\Delta\bar{H}^0_X - \tfrac{1}{2}\Delta\bar{H}^0_{EX} + \Delta\bar{H}^0_{24})s_2 \\ & - ({}^{[4]}W_{\text{FeMg}} - W_{2'\underline{5}} - W_{2\underline{5}'} + W_{2'2} + W_{1'5} + W_{15'} \\ & \quad + W_{\underline{45}'} - W_{45'} - W_{1'1} - \tfrac{1}{2}\Delta\bar{H}^0_{X'} - \tfrac{1}{2}\Delta\bar{H}^0_{EX} \\ & \quad + \Delta\bar{H}^0_{24} - \Delta\bar{H}^0_{25})s_4 \\ & + ({}^{[4]}W_{\text{FeMg}} + \tfrac{1}{2}\Delta\bar{H}^0_X)X_2 \\ & - ({}^{[4]}W_{\text{FeMg}} - \tfrac{1}{2}\Delta\bar{H}^0_{EX} - \tfrac{1}{2}\Delta\bar{H}^0_{X'} + \Delta\bar{H}^0_{24})X_3 \\ & - ({}^{[4]}W_{\text{FeMg}} + W_{14} - W_{2\underline{4}})X_4 \\ & - (\Delta\bar{H}^0_{25} + W_{2'\underline{5}} - W_{1'5} + W_{1'1} - W_{2'2})X_5 \\ = & (W_{3'\underline{4}} + W_{13'} - W_{3'4} - W_{2\underline{3}'})X_3. \end{aligned} \tag{21}$$

In this expression, $\Delta\bar{H}^0_{21}$ and $\Delta\bar{S}^0_{21}$ are the standard state enthalpy and entropy differences, respectively, between $MgAl_2O_4$ and $FeAl_2O_4$ in their inverse cation ordering states (Sack and Ghiorso, 1991), and s_1, s_2, and s_4 are given by solution of the conditions of homogeneous equilibrium (general expressions provided in Table 5). It should be noted that once calibrated, Equation 21 provides the basis for a general spinel-olivine geothermometer, which may be used to estimate equilibration temperatures for all spinel-olivine pairs of petrological interest.

Various data bearing on the calibration of Fe-Mg partitioning between olivine and $(Fe,Mg)(Al,Cr,Fe^{3+})_2O_4$-$(Fe,Mg)_2TiO_4$ are displayed in Figure 5. We note that the calibration for $\bar{Q}^*_{\text{Al-Cr}}$ is within analytical uncertainty of all such constraints and that it has been achieved utilizing a value for the parameter sum $(W_{3'\underline{4}} + W_{13'} - W_{3'4} - W_{2\underline{3}'})$ near the lower limit of the range permitted by the data displayed in Figure 4. We further note that to achieve this result it has been necessary to lower slightly the estimate for $\Delta\bar{H}^0_{24}$ and make other very minor adjustments in a few related parameters in the model of Sack and Ghiorso (1991). Although the value of $\Delta\bar{H}^0_{24}$ utilized by Sack and Ghiorso (1991; 28.5 kJ/gfw) is appropriate for the comparison of Fe-Mg partitioning relations between olivine and aluminate, ferrite, and titanate spinels, it leads to slight but consistent underestimates of $\bar{Q}^*_{\text{Al-Cr}}$ for mixed Ti-rich $(Fe,Mg)(Al,Fe^{3+})_2O_4 - (Fe,Mg)_2TiO_4$ and (Fe,Mg)-$(Al,Cr,Fe^{3+})_2O_4 - (Fe,Mg)_2TiO_4$. This discrepancy is remedied by adjusting $\Delta\bar{H}^0_{24}$ downward by about 2 kJ/gfw and refining related parameters (Tables 4 and 6) to ensure that the remaining constraints of phase equilibrium, cation ordering, and standard state summarized here and by Sack and Ghiorso (1991) continue to be satisfied. The resulting calibration yields values of $\bar{Q}^*_{\text{Ti}}$ (Sack and Ghiorso, 1991) that are slightly lower than those appropriate for the most Fe-rich and Mg-rich $(Fe,Mg)_2TiO_4$ reported by Hill and

TABLE 5. Conditions for homogeneous equilibrium

$$\left(\frac{\partial\bar{G}}{\partial s_1}\right)$$

$$\begin{aligned} 0 = & RT\ln\left[\frac{(X_2 + s_1)(2 - X_2 - 2X_3 + s_1 - 2s_2 - 2s_4)}{(X_2 - s_1)(2X_3 + 2X_4 - X_2 - s_1 + 2s_2 + 2s_4)}\right] + \tfrac{1}{2}(\Delta\bar{G}^0_X + \Delta\bar{G}^0_{EX}) + (\Delta\bar{G}^0_{24} + W_{2\underline{4}} - W_{14} - {}^{[6]}W_{\text{FeMg}}) + (\bar{G}^0_X - {}^{[4]}W_{\text{FeMg}} - {}^{[6]}W_{\text{FeMg}})s_1 \\ & + ({}^{[4]}W_{\text{FeMg}} + {}^{[6]}W_{\text{FeMg}} - \Delta\bar{G}^0_X + W_{1'1} - W_{2'2})s_2 + ({}^{[4]}W_{\text{FeMg}} + {}^{[6]}W_{\text{FeMg}} - \Delta\bar{G}^0_X - W_{1'1} + W_{2'2} + W_{1'5} - W_{15'} - W_{2'\underline{5}} - W_{2\underline{5}'})s_4 \\ & + ({}^{[6]}W_{\text{FeMg}} - {}^{[4]}W_{\text{FeMg}})X_2 + ({}^{[4]}W_{\text{FeMg}} + {}^{[6]}W_{\text{FeMg}} - \Delta\bar{G}^0_X + W_{13'} - W_{2\underline{3}'})X_3 + ({}^{[4]}W_{\text{FeMg}} - W_{2\underline{4}} + W_{14} - \Delta\bar{G}^0_{24})X_4 \\ & + \tfrac{1}{2}(\Delta\bar{G}^0_{EX} - \Delta\bar{G}^0_{X'})X_4 + (W_{1'1} - W_{2'2} + W_{2'\underline{5}} - W_{1'5})X_5 \end{aligned}$$

$$\left(\frac{\partial\bar{G}}{\partial s_2}\right)$$

$$\begin{aligned} 0 = & RT\ln\left[\frac{(1 - X_3 - X_4 - X_5 + s_2)(X_3 + X_4 - \frac{X_2}{2} - \frac{s_1}{2} + s_2 + s_4)}{(1 - X_3 - X_4 - X_5 - s_2)(1 - \frac{X_2}{2} - X_3 + \frac{s_1}{2} - s_2 - s_4)}\right] + (W_{1'1} + \Delta\bar{G}^*_{1'1}) + \tfrac{1}{2}(W_{1'1} - W_{2'2} + {}^{[4]}W_{\text{FeMg}} + {}^{[6]}W_{\text{FeMg}} - \Delta\bar{G}^0_X)s_1 \\ & - 2W_{1'1}s_2 + (W_{15} + W_{1'5'} - W_{1'5} - W_{15'})s_4 + \tfrac{1}{2}({}^{[4]}W_{\text{FeMg}} - {}^{[6]}W_{\text{FeMg}} - \Delta\bar{G}^0_{EX} + W_{1'1} - W_{2'2})X_2 + (\Delta\bar{G}^0_{24} + W_{2'\underline{4}} - W_{1'4})X_2 \\ & + (W_{1'3'} - W_{13'} - W_{1'1})X_3 + (W_{1'4} - W_{14} - W_{1'1})X_4 + (W_{1'5} - W_{15} - W_{1'1})X_5 \end{aligned}$$

$$\left(\frac{\partial\bar{G}}{\partial s_4}\right)$$

$$\begin{aligned} 0 = & RT\ln\left[\frac{(X_5 + s_4)(2X_3 + 2X_4 - X_2 - s_1 + 2s_2 - 2s_4)}{(X_5 - s_4)(2 - X_2 - 2X_3 + s_1 - 2s_2 - 2s_4)}\right] + (\Delta\bar{G}^*_{5'5} + W_{15'} - W_{15}) \\ & + \tfrac{1}{2}({}^{[4]}W_{\text{FeMg}} + {}^{[6]}W_{\text{FeMg}} + W_{2'2} - W_{1'1} - \Delta\bar{G}^0_X + W_{1'5} + W_{15'} - W_{2'\underline{5}} - W_{2\underline{5}'})s_1 + (W_{15} + W_{1'5'} - W_{1'5} - W_{15'})s_2 \\ & - 2W_{5'5}s_4 + \tfrac{1}{2}({}^{[4]}W_{\text{FeMg}} - {}^{[6]}W_{\text{FeMg}} + W_{2'2} - W_{1'1} - \Delta\bar{G}^0_{EX} + W_{15'} + W_{1'5} - W_{2'\underline{5}} - W_{2\underline{5}'})X_2 + (\Delta\bar{G}^0_{24} - \Delta\bar{G}^0_{25} + W_{\underline{45}'} - W_{45'})X_2 \\ & + (W_{3'5'} - W_{3'5} + W_{15} - W_{15'})X_3 + (W_{15} + W_{45'} - W_{45} - W_{15'})X_4 + (W_{5'5} + W_{15} - W_{15'})X_5 \end{aligned}$$

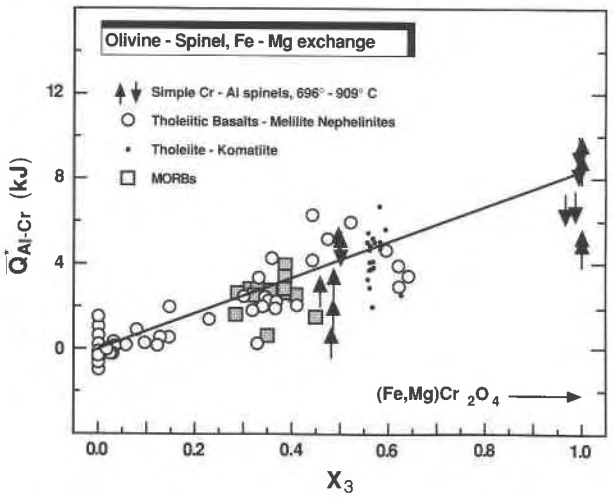

Fig. 5. Calibration for $\overline{Q}^*_{Al\text{-}Cr}$ (Eq. 21) compared with experimental and petrological constraints. Tips of arrows indicate values of $\overline{Q}^*_{Al\text{-}Cr}$ calculated from the results of exchange experiments for Fe-Mg between olivine and aluminate-chromite spinels at 696–909 °C (Engi, 1983). Arrows indicate the direction of change of $\overline{Q}^*_{Al\text{-}Cr}$ during a given experiment. Only the tightest reversal brackets for $X^{Ol}_{Fo} \leq 0.97$ and $X_3 > 0$ are shown; results of Cr-absent experiments are considered by Sack and Ghiorso (1991). Circles indicate spinel-olivine pairs from the melting and crystallization experiments of Sack (1982), Sack et al. (1987b), and Gee and Sack (1988). Shaded boxes represent values of $\overline{Q}^*_{Al\text{-}Cr}$ calculated for spinel-olivine pairs in glassy lavas from seamounts adjacent to the East Pacific Rise (Allan et al., 1987, 1988, 1989) and the Tuzo Wilson seamounts (Allan, personal communication) employing temperatures estimated by the authors. Dots indicate the experimental results of Murck and Campbell (1986). The diagonal line denotes the calibration of $\overline{Q}^*_{Al\text{-}Cr}$ based on the values of the thermodynamic parameters given in Tables 4 and 6. This line has zero intercept and a slope corresponding to the parameter sum $(W_{3'4} + W_{13'} - W_{3'4} - W_{23'})$.

Sack (1987). We emphasize that the resulting inconsistency pertains only to end-member titanate spinels in which short-range ordering is a complicating factor.

Standard state properties

In this section we derive internally consistent values for the thermodynamic properties of the end-member components $MgCr_2O_4$ (picrochromite) and $FeCr_2O_4$ (chromite). In addition, we update the end-member properties of the Cr-absent components reported by Sack and Ghiorso (1991). The recommended set of end-member thermodynamic properties to be used in conjunction with the solution parameters reported in Table 4 are provided in Tables 6a, 6b, and 6c. They are consistent with the thermodynamic data of Berman (1988) and our previously published solution theory for olivine, orthopyroxenes and rhombohedral oxides (Sack and Ghiorso, 1989, Ghiorso, 1990a).

Picrochromite ($MgCr_2O_4$)

Low-temperature heat capacity measurements have been reported by Shomate (1944; 54–296 K) and high-temperature heat content determinations have been provided by Naylor (1944; 387–1783 K).These experimental results were combined and fitted, according to the methods outlined in Berman and Brown (1985), to yield the heat capacity parameterization reported in Table 6a. The expression reproduces the data over the temperature range 250–1780 K with an average absolute deviation of less than 0.10%.

The adopted reference-state entropy of picrochromite (see Table 6b) is taken from Shomate (1944) and represents a smooth extrapolation to 0 K without inclusion of magnetic or structural ordering contributions. The zero-point entropy is assumed to be zero (consistent with a normal cation distribution down to 0 K). Subsequent to Shomate's (1944) experimental study, it has been shown that $MgCr_2O_4$ undergoes a paramagnetic-antiferromagnetic transition at ~16 K and a further magnetic transformation to a helicoidal spin ordering arrangement at ~13 K (Shaked et al., 1970). The maximum entropy that might result from these magnetic transitions is 2 R ln 4 (23.052 J/K), but the actual contribution could be less if the structure fails to develop the full long-range magnetic

TABLE 6A. Standard state thermodynamic properties

	k_0	k_1 (×10⁻²)	k_2 (×10⁻⁵)	k_3 (×10⁻⁷)	T_λ	L_1 (×10²)	L_2 (×10⁵)	$\Delta_f H$
$FeAl_2O_4$* (hercynite)	235.190	−14.370	−46.913	64.564				
$MgAl_2O_4$** (spinel)	235.90	−17.666	−17.104	4.062				
$FeCr_2O_4$† (chromite)	236.874	−16.796	0.000	−16.765				
$MgCr_2O_4$† (picrochromite)	201.981	−5.519	−57.844	57.729				
Fe_2TiO_4** (ulvöspinel)	249.63	−18.174	0.000	−5.453				
Mg_2TiO_4** (cubic phase)	226.11	−13.801	−17.011	4.128				
Fe_3O_4** (magnetite)	207.93	0.000	−72.433	66.436	848	−19.502	61.037	1565
$MgFe_2O_4$** (magnesioferrite)	196.66	0.000	−74.922	81.007	665	15.236	−53.571	931
298 K < T < T_λ	$C_P = k_0 + k_1T^{-0.5} + k_2T^{-2} + k_3T^{-3} + T(L_1 + L_2T)^2$							
T_λ < T	$C_P = k_0 + k_1T^{-0.5} + k_2T^{-2} + k_3T^{-3}$							

Note: Lattice and magnetic heat capacity functions (C_P) for temperatures greater than 298 K and pressures of 10^5 Pa.
* Estimated from algorithms in Berman and Brown (1985), with k_0 adjusted to agree with the 298.15 K value reported by King (1956).
** Berman and Brown (1985).
† Fitted to the Berman and Brown (1985) form from data provided by Naylor (1944) and Shomate (1944).

TABLE 6B. Standard state thermodynamic properties

	Adopted value (J/K)	Reported value (J/K)	Uncertainty (J/K)		Inverse (J/K)		Entropy at 0 K (J/K)	Ordering (J/K)
$FeAl_2O_4$ (hercynite)	115.362	106.270[A]	0.84	$\overline{S}_1^*$	115.358	$\overline{S}_1^0 - \overline{S}_1^*$	0.000	0.004
$MgAl_2O_4$ (spinel)	84.535[B]	80.584[C]	0.42	$\overline{S}_2^*$	84.320	$\overline{S}_2^0 - \overline{S}_2^*$	0.000	0.215
$FeCr_2O_4$ (chromite)	142.676	146.020[D]	1.67	$\overline{S}_3^*$	154.202	$\overline{S}_3^0 - \overline{S}_3^*$	11.526	
$MgCr_2O_4$ (picrochromite)	106.020	106.020[D]	0.84		117.546		11.526	
Fe_2TiO_4 (ulvöspinel)	185.447[E]	163.176[F]	2.51	$\overline{S}_4^*$	173.921	$\overline{S}_4^0 - \overline{S}_4^*$	11.526	
Mg_2TiO_4 (cubic phase)	120.170	103.596	0.63		108.644		11.526	
Fe_3O_4 (magnetite)	146.114[B]	146.147[G]	0.84	$\overline{S}_5^*$	146.111	$\overline{S}_5^0 - \overline{S}_5^*$	0.000	0.003
$MgFe_2O_4$ (magnesioferrite)	122.765	118.407[H]	0.84		122.662		0.000	0.103

Note: Entropy at 298.15 K and 10^5 Pa.
[A] King (1956). C_P measured from 51 to 298 K and extrapolated to 0 K assuming no low-temperature magnetic transitions.
[B] Berman (1988). See text.
[C] King (1955). C_P measured from 51 to 298 K and extrapolated to 0 K assuming no low-temperature magnetic transitions.
[D] Shomate (1944).
[E] Reported value + 2R ln 2 + residual low-temperature magnetic entropy.
[F] Todd and King (1953). C_P measured from 51 to 298 K and extrapolated to 0 K assuming no low-temperature magnetic transitions below those detected at 56 K and 99.1 K (magnetostriction effect and the paramagnetic-antiferromagnetic transformation).
[G] Westrum and Grønvold (1969). C_P measured from 5 to 298 K and extrapolated to 0 K. The reported value has no zero point addition.
[H] King (1954). C_P measured from 51 to 298 K and extrapolated to 0 K assuming no low-temperature magnetic transitions. The reported value has no zero point addition.

order even at low temperatures (e.g., McGuire et al., 1952). [The maximum magnetic contribution to the entropy is given by R ln $(2s + 1)$, where s is the sum of the unpaired spins of the electrons that participate in the development of magnetic order (Gopal, 1966). The Cr^{3+} ion has three such unpaired d-electrons; hence s is equal to 3/2.] Without detailed adiabatic calorimetry below 50 K, the question of the magnetic contribution to the reference-state entropy of picrochromite remains unresolved.

The reference-state enthalpy is taken from Robie et al. (1978), who adopt the value of Parker et al. (1971). The origin and uncertainty of this number are unknown.

Chromite ($FeCr_2O_4$)

The low-temperature adiabatic calorimetry measurements of Shomate (1944; 53–296 K) are combined with the high-temperature heat content measurements of Naylor (1944; 386–1787 K) to generate the equation for heat capacity reported in Table 6a. The fitting procedure is described by Berman and Brown (1985), and the equation

TABLE 6C. Standard state thermodynamic properties

	Adopted value (kJ)	Reported value (kJ)	Uncertainty (kJ)	Normal (kJ)		Inverse (kJ)	Ordering (kJ)
$FeAl_2O_4$ (hercynite)	−1947.681	−1966.480*	8.500	−1947.682	$\overline{H}_1^*$	−1911.281	0.001
$MgAl_2O_4$ (spinel)	−2300.313	−2302.000**	2.700	−2300.369	$\overline{H}_2^*$	−2281.959	0.056
$FeCr_2O_4$ (chromite)	−1445.490			−1445.490	$\overline{H}_3^*$	−1416.202	0.000
$MgCr_2O_4$ (picrochromite)	−1783.640	−1783.640†	8.370	−1783.640		−1774.017	0.000
Fe_2TiO_4 (ulvöspinel)	−1488.500				$\overline{H}_4^*$	−1488.500	
Mg_2TiO_4 (cubic phase)	−2161.998	−2164.383‡	6.726			−2161.998	
Fe_3O_4 (magnetite)	−1117.403	−1117.403*		−1091.254	$\overline{H}_5^*$	−1117.404	0.001
$MgFe_2O_4$ (magnesioferrite)	−1406.465	−1428.420†	1.841	−1409.367		−1406.438	0.027

Note: Enthalpy of formation from the elements at 298.15 K and 10^5 Pa.
* Wagman et al. (1969).
** Shearer and Kleppa (1973).
† Robie et al. (1978).
‡ Stull and Prophet (1971).

reproduces the data over the temperature range 250–1790 K with an average absolute deviation of less than 0.20%.

Shomate (1944) reports an estimate for the reference-state entropy of chromite (Table 6b). The value was obtained by the usual method of extrapolating a smooth extension of the measured C_P curve to 0 K and includes energetic contributions from two nonnormal sources. A lambdalike C_P anomaly, which develops over the range 90–140 K, results in an entropy contribution of 2.37 J/K·gfw and is probably related to the cubic-tetragonal phase transition (Francombe, 1957; Shirane et al., 1964). The C_P anomaly at lower temperature, which peaks at 75 K, coincides nicely with the measured Néel temperature of 80 K (Shirane et al., 1964). However, the entropy effect (over the range 50–80 K) associated with this paramagnetic-antiferromagnetic transition is only 0.75 J/K·gfw (Shomate, 1944). This suggest that the majority of the magnetic entropy (up to 2 R ln 4 + R ln 5; 36.433 J/K·gfw) is either not developed at lower temperatures or is associated with the transformation from collinear to helicoidal spin that is known to occur at ~35 K (Shirane et al., 1964). Although the calorimetric data do not allow these issues to be resolved, an independent estimate for the reference-state entropy of chromite can be found by recognizing that the relation

$$\overline{S}^0_{FeCr_2O_4} = \overline{S}^0_{MgCr_2O_4} - 2\Delta\overline{S}^0_{24} - \Delta\overline{S}^0_{21} \qquad (22)$$

must hold as a consequence of our formulation for the vibrational Gibbs energy of spinel solutions. From the tabulated expressions of heat capacity for picrochromite and chromite, and our calibration of the exchange of Fe^{2+}-Mg between chromian spinel and olivine (Figs. 4 and 5), we arrive at an internally consistent estimate of 142.676 J/K·gfw for the reference-state entropy of chromite. This number is at the lower limit of the 2σ uncertainty of the value reported by Shomate (1944). Our estimate is subject to the same absolute uncertainty as that ascribed to picrochromite.

An expression similar to Equation 22 relates the reference-state enthalpy of formation of picrochromite to that of chromite. Simplification of $\overline{G}^*$ yields

$$\begin{aligned}\Delta\overline{H}^0_{f,FeCr_2O_4} = {} & \Delta\overline{H}^0_{f,MgCr_2O_4} - 2\Delta\overline{H}^0_{24} - \Delta\overline{H}^0_{21} \\ & + (W_{14} + W_{2\underline{3}'} + W_{3'4}) \\ & - (W_{13'} + W_{2\underline{4}} + W_{3'\underline{4}})\end{aligned} \qquad (23)$$

which results, by means of analysis of equilibria involving exchange of Fe^{2+} and Mg between olivine and spinel (Figs. 4 and 5), in an internally consistent estimate of $\Delta\overline{H}^0_{f,298K,1bar}$ for $FeCr_2O_4$. This value is adopted and is reported in Table 6c.

Aluminates, titanates, and ferrites

Internally consistent thermodynamic properties for Fe^{2+}-Mg aluminate, titanate, and ferrite end-member spinels are derived by Sack and Ghiorso (1991). Their analysis is based on values for the standard-state properties of spinel ($MgAl_2O_4$) and magnetite (Fe_3O_4) derived by Berman (1988), and on Ghiorso's (1990a) estimate for the thermodynamic properties of ulvöspinel (Fe_2TiO_4). In combination with their solution parameters, these reference properties of the end-members permit Sack and Ghiorso (1991) to derive values for the reference-state entropy and enthalpy of formation of hercynite ($FeAl_2O_4$), $MgFe_2O_4$, and Mg_2TiO_4. In this paper we have made minor revisions to the solution parameters for the aluminate-titanate-ferrite-spinel subsystem. Consequently, revised estimates for the reference-state entropies and enthalpies of formation of hercynite, Mg_2TiO_4, and $MgFe_2O_4$ are reported in Table 6. Methods of obtaining these estimates are discussed in our previous paper. A convenient summary of the remaining end-member thermodynamic properties is also provided in Table 6. These values are taken directly from Table 7 of Sack and Ghiorso (1991).

Discussion

Several features of the calibration of the thermodynamic properties of chromian spinels are noteworthy. The first concerns data on coexisting Cr- and Ti-rich spinels found in lunar basalts (e.g., Agrell et al., 1970; Champness et al., 1971; Taylor et al., 1971). These have compositions that plot near the thermal minima in the calculated miscibility gaps for $FeAl_2O_4$-Fe_2TiO_4-$FeCr_2O_4$ and $MgAl_2O_4$-Mg_2TiO_4-$MgCr_2O_4$ (Figs. 3a and 3b). We speculate that this coincidence may reflect a similar feature in the solidus surface for the relevant lunar basalt liquids. An additional curious feature of our calibration is the sigmoidal shape associated with calculated distribution coefficients for the Fe-Mg exchange between olivine and aluminate-chromite spinels, and olivine and chromite-ferrite spinels (Figs. 6 and 7). This feature is especially evident for chromite-ferrite spinels (Fig. 6) and bears a remarkable parallel with the systematics exhibited by distribution coefficients for the Fe-Zn exchange between sphalerite and argentian tetrahedrite-tennantite fahlores (cf. O'Leary and Sack, 1987; Sack et al., 1987a; Sack, 1991). In tetrahedrite fahlores [$\approx (Cu,Ag)_{10}(Fe,Zn)_2Sb_4S_{13}$; e.g., Spiridonov, 1984] the Fe/(Fe + Zn) ratio exhibits a pronounced sigmoidal dependence on Ag/(Ag + Cu) ratio at fixed Fe/(Fe + Zn) ratio in sphalerite, and the local maxima and minima correspond to similar features in cell volumes, reflectivities, and $Ag(Cu)_{-1}$ exchange potentials (e.g., Indolev et al., 1971; Riley, 1974; Paar et al., 1978; Ebel and Sack, 1989). This fahlore effect has been ascribed to a change in Ag site preference with increasing ratio of Ag/(Ag + Cu). The parallel feature in $(Fe,Mg)(Cr,Fe^{3+})_2O_4$ is certainly caused by the change of site preference of Fe^{3+} that is associated with increasing ratios of $Cr/(Cr + Fe^{3+})$ in $FeCr_2O_4$-Fe_3O_4 (e.g., Fig. 1). In this case there is also a parallel between the fahlore effect and room temperature volume-composition systematics (e.g., Francombe, 1957; Robbins et al., 1971).

Despite this complication, it is noteworthy that the calculated curves for Fe-Mg distribution coefficients (Figs. 6 and 7) yield temperatures that are in general accord with those estimated for metamorphosed ultramafic rocks

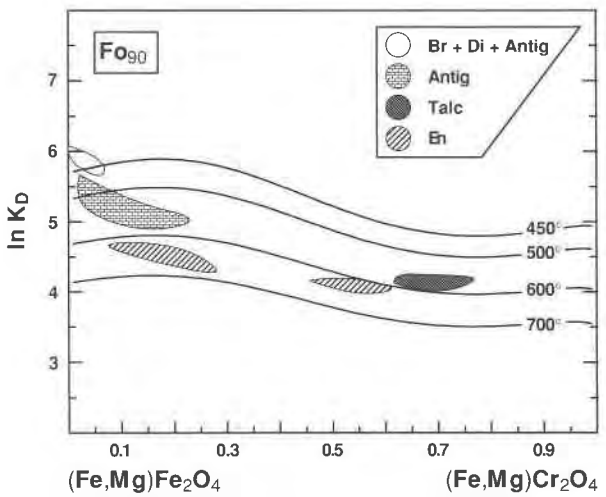

Fig. 6. Isotherms of ln K_d [$K_d \equiv (X^{Ol}_{Fo} X^{Sp}_{bulkFe^{2+}})/(X^{Ol}_{Fa} \cdot X^{Sp}_{bulkMg^{2+}})$] for the Fe-Mg exchange between olivine ($X^{Ol}_{Fo} = 0.90$) and ferrite-chromite spinels, compared with petrological data for metamorphosed serpentinites (Evans and Frost, 1975, their Fig. 7). Shaded areas outline portions of the graph in which there are dense populations of data points for the indicated prograde mineral assemblages. Abbreviations are as follows: Br = brucite; Di = diopside; Antig = antigorite; En = enstatite.

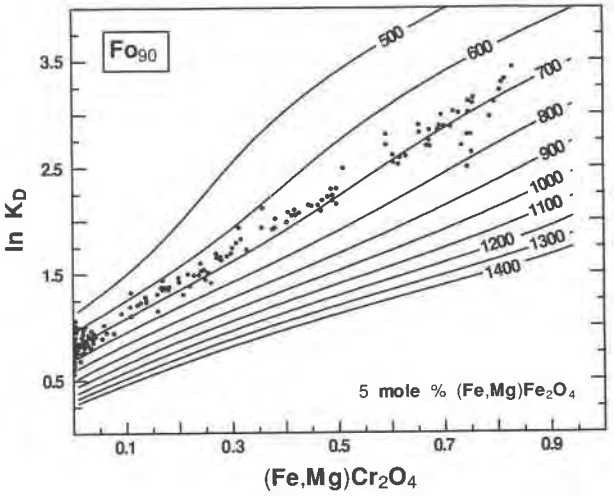

Fig. 7. Isotherms of ln K_d [$K_d \equiv (X^{Ol}_{Fo} X^{Sp}_{bulkFe^{2+}})/(X^{Ol}_{Fa} \cdot X^{Sp}_{bulkMg^{2+}})$] for the Fe-Mg exchange between olivine ($X^{Ol}_{Fo} = 0.90$) and aluminate-chromite spinels (with 5 mol% ferrite component) compared with petrological data for metamorphosed chlorite-enstatite-olivine rocks (Evans and Frost, 1975, their Fig. 6).

on the basis of mineral assemblages (e.g., Evans and Frost, 1975). The comparison for ferrichromite spinel + olivine assemblages is especially compelling in that Evans and Frost (1975) noted that there is a minimum in the distribution coefficient at intermediate ratios of Cr/(Cr + Fe^{3+}) (Fig. 6). The maxima associated with calculated curves of Fe-Mg distribution coefficients at low ratios of Cr/(Cr + Fe^{3+}) is probably not evident from the natural assemblages because they are distinctly polythermal. The calculated curves for the Fe-Mg exchange between olivine and $(Fe,Mg)(Al,Cr)_2O_4$ (Fig. 7) agree with the correlation established for 700°C by Evans and Frost (1975) for contact metamorphosed serpentinites in which chlorite was thermally decomposed.

A potentially informative application of our model pertains to the analysis of phase relations of chromian spinels over the temperature range appropriate for the upper greenschist-amphibolite facies of metamorphism, 450–650 °C. In Figures 8–10 we present a series of diagrams to illustrate predicted phase relations within $(Fe,Mg)(Al,Cr,Fe^{3+})_2O_4$ under these conditions. Phase relations within this quaternary, the so-called spinel prism, are undoubtedly complex, as evidenced by extensive miscibility gaps in $(Fe,Mg)(Al,Fe^{3+})_2O_4$ (e.g., Turnock and Eugster, 1962; Sharma et al., 1973; Lehmann and Roux, 1986) and conflicting interpretations regarding miscibility relations in other subsystems of the prism (e.g., Cremar, 1969; Evans and Frost, 1975). As can be seen from Figure 8, the critical temperatures associated with gaps in the binary spinels $Fe(Al,Cr)_2O_4$, $Mg(Al,Cr)_2O_4$, $Fe(Cr,Fe^{3+})_2O_4$, and $Mg(Cr,Fe^{3+})_2O_4$ are 250–450 °C lower than those associated with $Fe(Al,Fe^{3+})_2O_4$ and

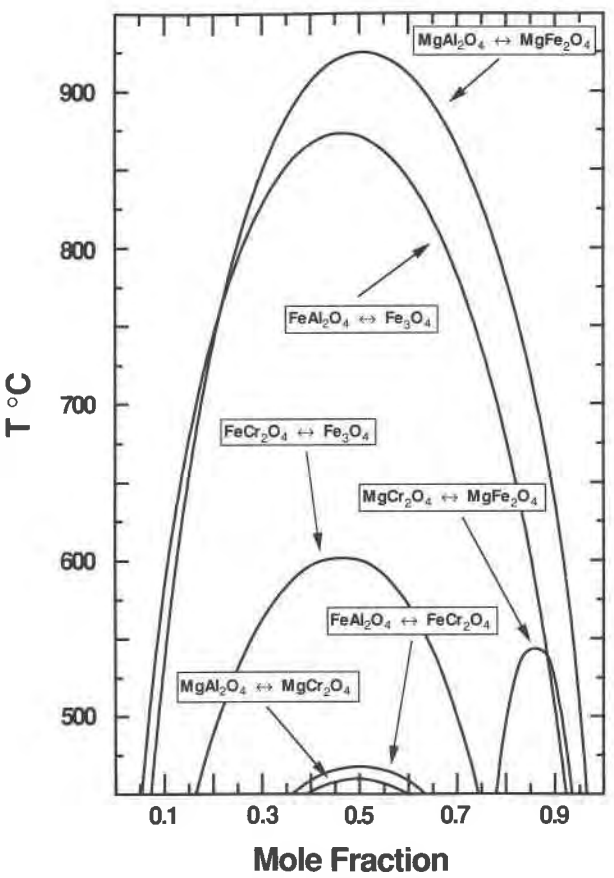

Fig. 8. Comparison of calculated miscibility gaps for the Fe^{2+} and Mg^{2+} binaries of the spinel prism, $(Fe,Mg)(Al,Cr,Fe^{3+})_2O_4$. Labels indicate sense of the composition axes associated with individual binaries (e.g., $FeCr_2O_4 \leftrightarrow Fe_3O_4$ indicates that Fe_3O_4 is on the right hand side of the composition axis).

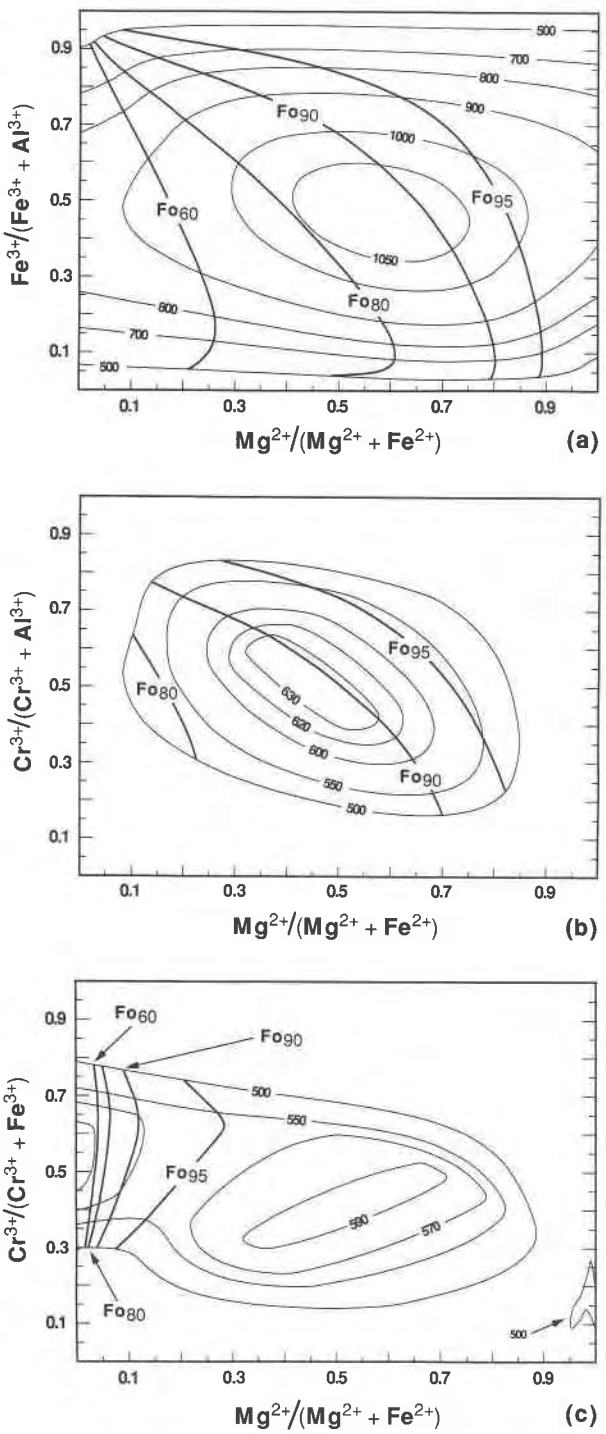

Fig. 9. Temperature-contoured miscibility gaps for Mg^{2+}-Fe^{2+}, 2-3 ternary spinels defining the sides of the spinel prism. The isotherms are overlain by contours of Mg/Fe ratios of coexisting olivine. The intersections of miscibility-gap isotherms with isopleths of olivine composition (labeled Fo_{60}, Fo_{80}, Fo_{90}, and Fo_{95}) define tie lines for coexisting spinels that are in Fe-Mg exchange equilibrium with this olivine. (**a**) Calculated 500, 700, 800, 900, 1000, and 1050 °C miscibility gaps for $(Fe,Mg)(Al,Fe^{3+})_2O_4$. (**b**) Calculated 500, 550, 600, 620, and 630 °C miscibility gaps for $(Fe,Mg)(Al,Cr)_2O_4$. (**c**) Calculated 500, 550, 570, and 590 °C miscibility gaps for $(Fe,Mg)(Cr,Fe^{3+})_2O_4$.

←

$Mg(Al,Fe^{3+})_2O_4$. According to our calculations, the miscibility gaps in $Fe(Al,Cr)_2O_4$ and $Mg(Al,Cr)_2O_4$ are very similar. Both have similar critical temperatures, are reasonably symmetric, and have fairly flat T-X profiles. In contrast, the calculated critical temperature for $Fe(Cr,Fe^{3+})_2O_4$ is distinctly higher than that for $Mg(Cr,Fe^{3+})_2O_4$. Both gaps have fairly steep T-X profiles, and the gap for $Mg(Cr,Fe^{3+})_2O_4$ is strongly asymmetric. The different senses of asymmetry exhibited by these binary spinels is almost certainly a reflection of differences in the degree of inversion exhibited by magnetite and magnesioferrite (e.g., Sack and Ghiorso, 1991).

We predict that the maxima associated with the critical curves for each of the ternaries comprising the sides of the spinel prism are at intermediate ratios of Fe/Mg (Fig. 9). The degree to which the maxima in the critical curves extend to higher temperatures than the consolutes in the constituent Fe^{2+} and Mg^{2+} binaries (Fig. 8) is primarily a function of the relative partitioning of Fe^{2+} and Mg^{2+} between coexisting spinels and reflects the nonideality associated with this substitution. It has been shown that this nonideality must be at least about 2 kJ/gfw at intermediate ratios of $Fe^{2+}/(Fe^{2+} + Mg^{2+})$ to be consistent with increased widths of gaps in ternary $(Fe,Mg)(Al,Fe^{3+})_2O_4$ and other data on activity-composition relations (e.g., Trinel-Dufour and Perrot, 1977; Shishkov et al., 1980; Lehmann and Roux, 1986; Sack and Ghiorso, 1989, 1991). In this ternary, the maximum in the critical curve is at a temperature between 150 and 200 °C higher than the consolutes in the constituent Fe and Mg binaries, and the miscibility gaps have their maximum widths where the differences in the ratios of $Fe^{2+}/(Fe^{2+} + Mg^{2+})$ of coexisting spinels are greatest. The maxima in the critical curves of $(Fe,Mg)(Al,Cr)_2O_4$ and $(Fe,Mg)(Cr,Fe^{3+})_2O_4$ extend to lower temperatures relative to the consolutes in their constituent Fe and Mg binaries because Fe^{2+} and Mg^{2+} are not as strongly partitioned between coexisting spinels in these ternary systems. The critical curve for $(Fe,Mg)(Cr,Fe^{3+})_2O_4$ exhibits a local maximum between two local minima, and it has a sigmoid shape. These features are illustrated in Figures 9a–9c by contours for both temperature and ratios of $Mg^{2+}/(Fe^{2+} + Mg^{2+})$ for spinel pairs that would coexist with several selected olivine compositions (Fo_{60}, Fo_{80}, Fo_{90}, and Fo_{95}).

It is convenient to use these olivine compositions to illustrate tie lines between coexisting Fe^{2+}-Mg^{2+} ternary spinels in Figures 9a–9c and to define the Fe-Mg exchange potentials for isothermal sections through the spinel prism. In Figures 10a–10e we have prepared a series of such isothermal pseudoternary sections and ternary diagrams to illustrate phase relations in the spinel prism

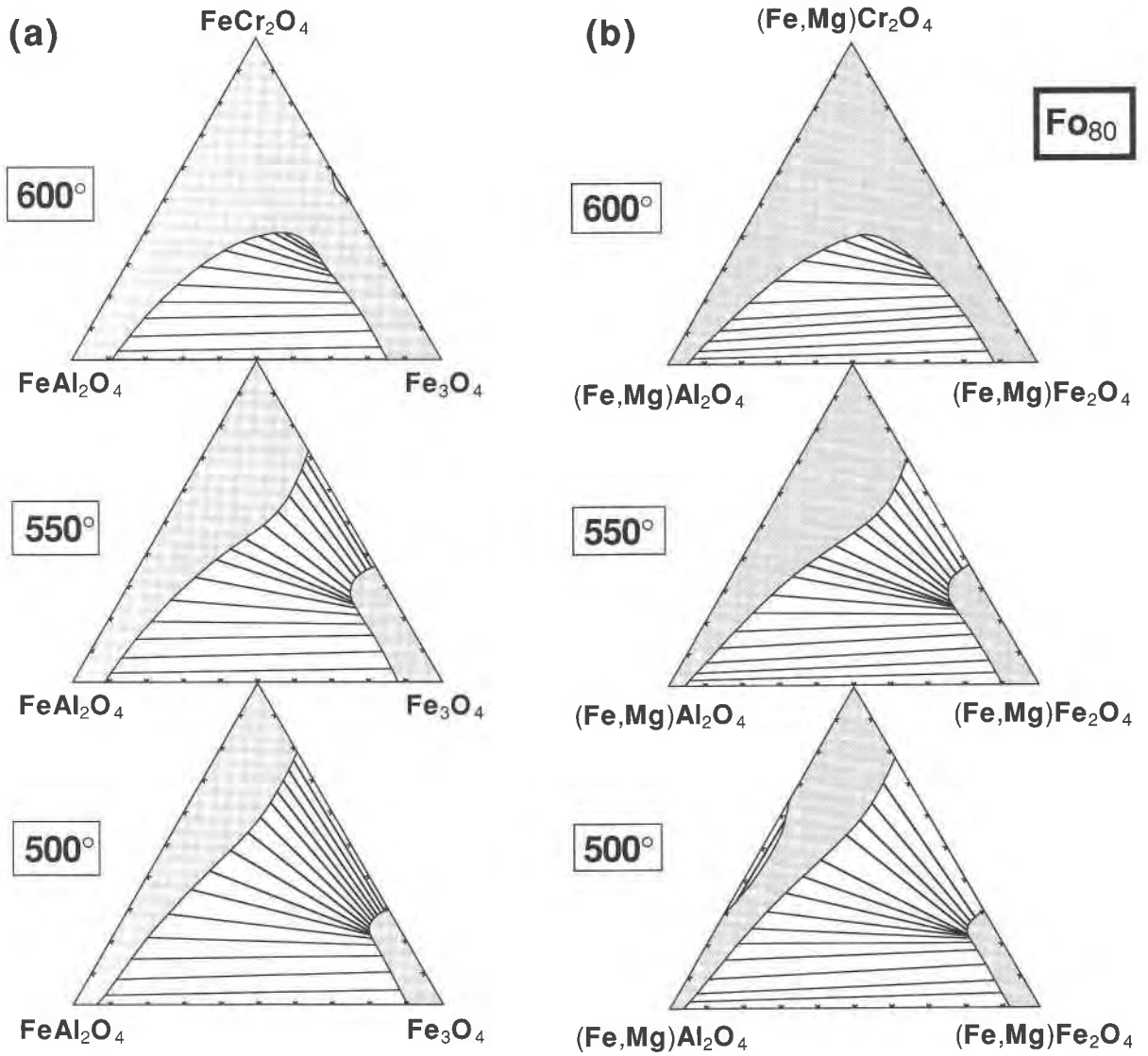

Fig. 10. Isothermal sections at 500, 550, and 600 °C through the spinel prism calculated for fixed Fe-Mg exchange potentials defined by olivine of various compositions. Shaded areas indicate fields of complete solid solution and solid lines denote tie lines between coexisting spinels. (**a**) Fo_0; (**b**) Fo_{80}.

over the temperature range 500–600 °C. Most of the features of these diagrams are readily predictable from the phase relations established for the sides of the prism (Figs. 9a–9c), although there are a few complications. Because the miscibility gaps in the bounding ternary system forming the front face of the prism are the only extensive ones over this entire temperature range, it follows that the most persistent feature of these pseudoternary and ternary diagrams is the two-phase region formed by the extension of the miscibility gaps of aluminate-ferrite spinels into the Cr-bearing system (Fig. 9a). With decreasing temperature this two-phase region becomes more extensive and its critical curve migrates toward the side of the prism that next displays immiscibility. Thus, in the case of the Fe base of the prism (Fig. 10a) and for the Fo_{80} and Fo_{95} sections (Figs. 10b and 10d, respectively), decreasing temperature first leads to the establishment of a continuous two-phase region connecting the miscibility gaps on the front and right hand faces of the prism. The temperatures along the associated critical curves are monotonic functions of composition, except for the basal section (Fig. 10a, top panel) in which the critical curve has a minimum near the magnetite-chromite binary. In each of these sections, the continuous two-phase region is established before it is intersected by the critical curves emanating from the left hand side of the prism to form a three-phase triangle. The latter curves have temperature minima in the sections for olivine with intermediate ratios of Fe/Mg (Figs. 10b, 10d). In the remaining interior section (Fo_{90}, Fig. 10c) and the Mg top of the prism (Fig. 10e), the critical curve governing the extension of the miscibility gaps of aluminate-ferrite spinels into the Cr-bearing sys-

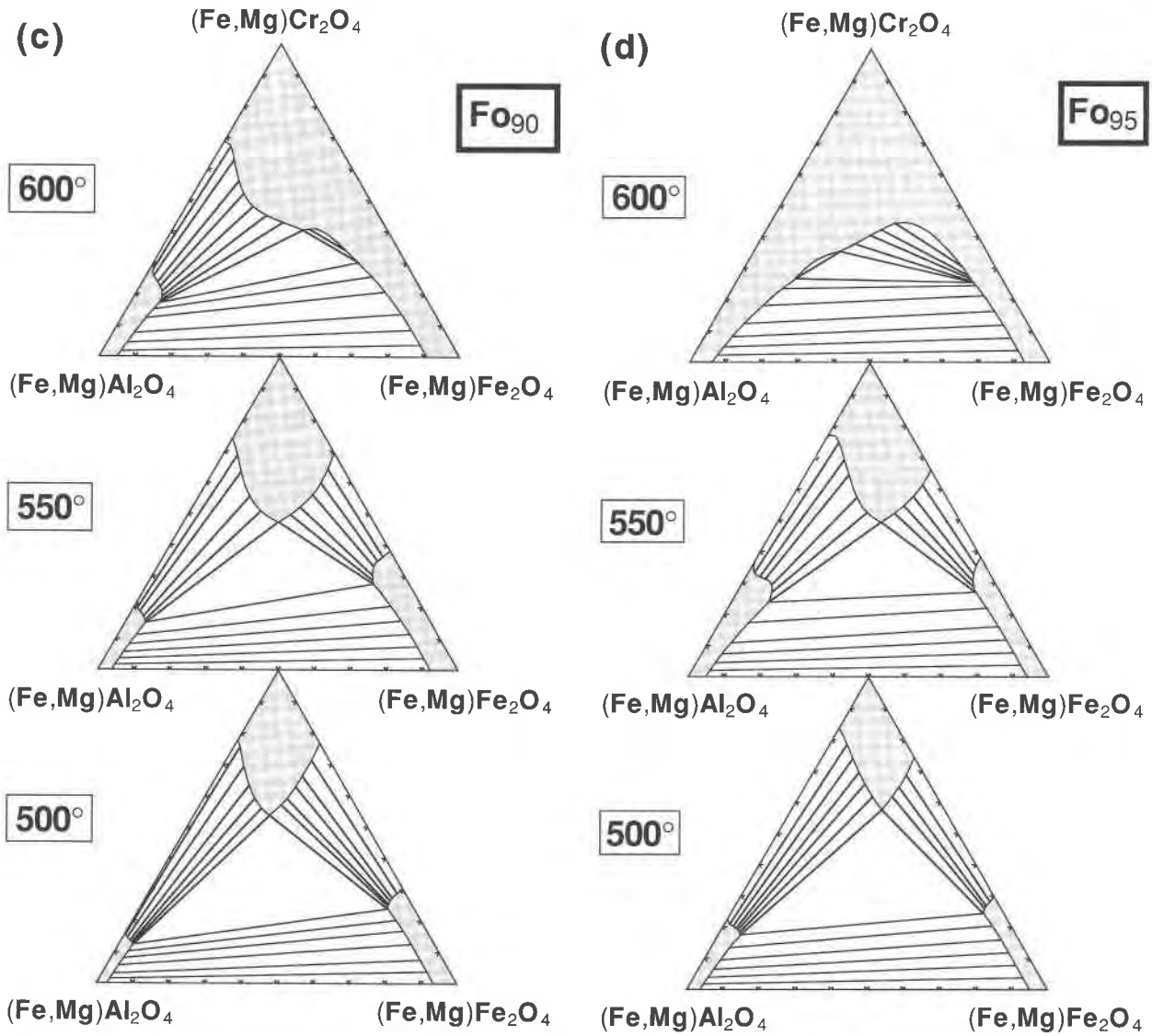

Fig. 10. (c) Fo_{90}; (d) Fo_{95}.

tem migrates toward the left side of the prism with decreasing temperature. In the Fo_{90} section (Fig. 10c), a continuous two-phase region is established between the front and left hand faces of the prism before it is intersected by the critical curves emanating from the right side of the prism, whereas in the Mg ternary (Fig. 10e) a three-phase triangle is developed before the critical curve intersects the left face of the prism. In both cases temperature minima are associated with the critical curves emanating from the right face of the prism.

It is noteworthy that our predicted miscibility gaps are in general accord with constraints from nature. They are, for example, in agreement with the observations of Muir and Naldrett (1973), who report evidence for unmixing of some of the originally homogeneous spinel from the Giant nickel mine, Hope, British Columbia. Their composition data and petrographic observations indicate that the miscibility gaps between aluminate and ferrite spinels extend to less than about 30 mol% $(Fe,Mg)Cr_2O_4$ component at the temperature at which unmixing ceased. Our calculated miscibility gaps agree with their inferences, given the temperatures we calculate for Fe-Mg exchange equilibrium between their reported exsolved pairs, 645 ± 24 °C ($Fo_{84.7}$–$Fo_{86.8}$). Support for our calculated miscibility gaps for $(Fe,Mg)(Cr,Fe^{3+})_2O_4$-rich spinels is also provided by the composition data for coexisting spinels in the metamorphosed chromite ores of Red Lodge, Montana (Loferski and Lipin, 1983) and in the gabbroic rocks and ores from the Ni-Cu mine of Kusså, Bergslagen, Sweden (Zakrzewski, 1989). Both report composition gaps between coexisting Cr^{3+}- and Fe^{3+}-rich spinels of similar widths and with tie lines of similar slopes to those cal-

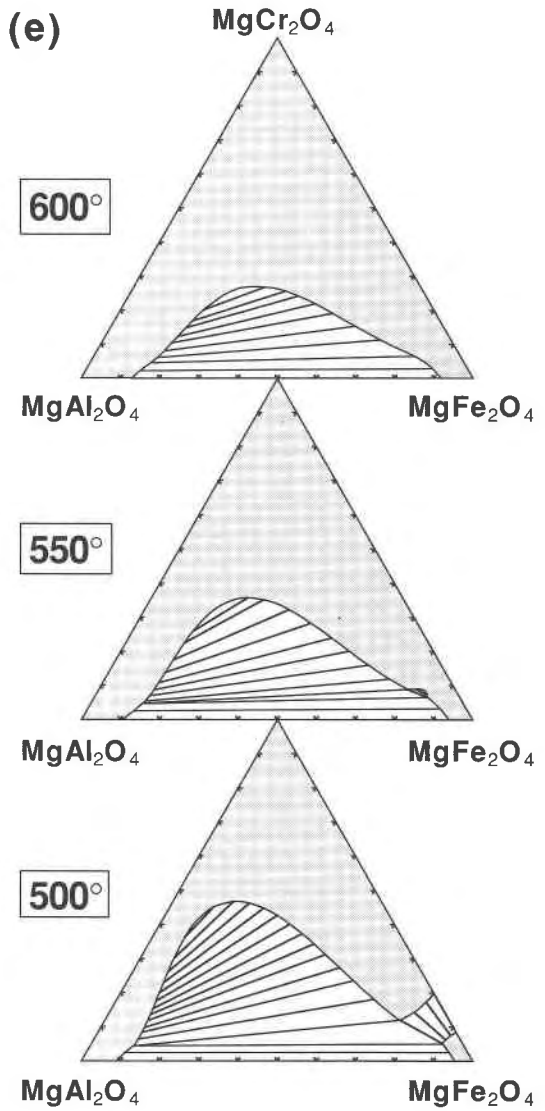

Fig. 10. (e) Fo_{100}.

culated for temperatures between 550 and 600 °C (Figs. 10c–10e; Loferski and Lipin, samples HP-14, LC-4, and SR-2; Zakrzewski, analyses 70–71). The chromite ores from Red Lodge experienced peak metamorphic temperatures of about 600 °C, during which the coarse exsolution features in the spinels presumably developed (Loferski and Lipin, 1983). There is the further complication that these coarse exsolution lamellae and their hosts also develop exceedingly fine secondary exsolution lamellae. Although temperatures calculated for Fe-Mg exchange equilibrium for average compositions of coexisting spinels are quite uncertain because of the large relative uncertainties in the MgO contents of the Fe^{3+}-rich spinels, they are consistent with metamorphic equilibration at temperatures in the 550–600 °C range and local, $Fe(Mg)_{-1}$ exchange potentials corresponding to $0.86 \leq X_{Fo}^{Ol} \leq 0.935$ (calculated for these temperatures from spinels with MgO > 7 wt%). Our model is also consistent with the composition data for chromian spinels in metamorphosed ultramafic rocks, if it is recognized that complex thermal histories and chemical zoning in polycrystalline grains (e.g., Zakrzewski, 1989) are possible complicating factors.

Two studies of Cr-bearing spinels in ultramafic rocks metamorphosed in the greenschist-amphibolite facies may be used to highlight difficulties associated with interpreting such materials. Evans and Frost (1975) determined the compositions of chromian spinel for various prograde metamorphic assemblages in alpine serpentinites. They inferred that ferrichromite solid solutions are stable down to temperatures of about 500 °C because they obtained microprobe analyses with intermediate ratios of $Cr^{3+}/(Cr^{3+} + Fe^{3+})$ for spinel in rocks of the greenschist facies and lower amphibolite facies. Although most of their composition data plot within the one-phase fields of the appropriate sections of the spinel prism (e.g., Figs. 9c, 10d), the composition data for spinel inferred to have intermediate ratios of $Cr^{3+}/(Cr^{3+} + Fe^{3+})$ in rocks containing olivine + antigorite do not (their Fig. 7). However, the inference that these compositions represent equilibrium single-phase spinel is problematic because they have distribution coefficients for Fe-Mg exchange between olivine and spinel that are comparable to or lower than those in rocks containing talc + olivine or enstatite + olivine. If they represented equilibrium, they would record temperatures at least 100 °C too high for the assemblage olivine + antigorite (cf. Figs. 6 and 7). Spinels in these rocks are often complexly zoned on an exceedingly fine scale. Individual analyses may not correspond to single crystals or to equilibrium compositions. Finally, their analyses of ferrichromites show a distinct bimodal distribution of ratios of $Cr^{3+}/(Cr^{3+} + Fe^{3+})$, which is broadly consistent with the predicted miscibility gaps (e.g., their Figs. 1 and 6).

Complex zoning within individual grains is not an uncommon feature of chromian spinels in metamorphosed ultramafic rocks. For example, Hoffman and Walker (1978) report such features in the chrome spinel in the East Dover ultramafic bodies from south-central Vermont. In these bodies chrome spinel has ubiquitous ferrichromite-ferrite overgrowths, the widths and characters of which are related to the degree of serpentinization. With increasing degree of serpentinization, olivine becomes progressively more magnesian ($Fo_{92.3-96.6}$), the spinel overgrowths become wider, and the ratios of Mg/(Mg + Fe) and Al/(Al + Cr) of the spinel cores increase. In the least serpentinized bodies, the spinel overgrowths consist of a thin rim of ferrichromite only. In the more serpentinized bodies, they are comprised of an inner zone of ferrichromite and an outer zone of magnetite. Based on these features, Hoffman and Walker (1978) postulate that the three spinels in these grains, an aluminous chromite [Cr/(Cr + Al) ≈ 0.58], a ferrichromite [Cr/(Cr + Fe^{3+}) ≈ 0.42], and a magnetite, were produced simultaneously as a result of serpentinization at temperatures

appropriate to the upper greenschist-epidote amphibolite facies. We note that our predicted phase relations (Figs. 9c, 10e) are inconsistent with three such spinels being in equilibrium under these conditions. By analysis of the Fe-Mg partitioning relations between these spinels and olivine, it may readily be shown that they were not. Although our Fe-Mg olivine-spinel exchange geothermometer (Eq. 21) yields similar temperatures for the cores and rims of spinel in the least altered ultramafic and in serpentinites of intermediate textural type (types 1 and 2, Table 1, Hoffman and Walker, 1978), it yields temperatures that decrease progressively from the cores to the rims for spinel in the most serpentinized ultramafics (type 3). The temperatures deduced for spinel in these first two types (>585 °C) are consistent with the absence of the appropriate miscibility gaps. However, only the first two of the calculated rim-core temperatures for the most serpentinized ultramafic (472, 483, and 412 °C for magnetite, ferrichromite, and chromian spinel, respectively) could correspond to the temperature of the serpentinization reaction; the other clearly indicates the absence of equilibrium among these three coexisting spinels.

Comments on model extension

Although our model provides a good approximation for activity-composition relations in multicomponent spinels and reproduces Fe-Mg partitioning between olivine and spinels with compositions of petrological interest over a wide range of temperatures, it has a few shortcomings that need to be addressed in future refinements. The most serious of these derives from our lack of consideration of the contribution of short-range cation ordering to the configurational entropy of the titanate spinels (e.g., Banerjee et al., 1967; Wechsler and Navrotsky, 1984; Sack and Ghiorso, 1991). This oversight may result in errors in some of the parameter values established from analysis of activity-composition constraints and miscibility-gap features in constituent Ti-bearing subsystems (e.g., Fe_3O_4-Fe_2TiO_4, $FeAl_2O_4$-Fe_2TiO_4, and $MgAl_2O_4$-Mg_2TiO_4). The most serious consequence for spinels of petrological relevance is that we have probably slightly overestimated the enthalpy of the Fe^{2+}-Fe^{3+} ordering reaction in Fe_3O_4 ($\Delta\overline{H}^*_{5'5}$). Our value for this enthalpy, 26.2 kJ/gfw (Table 5), is about 20% larger than that which would produce optimum agreement with room temperature cation ordering constraints and volume-composition systematics in Fe_3O_4-$FeCr_2O_4$ spinels (Eq. 10; Fig. 1). It is noteworthy that the lower estimate ($\Delta\overline{H}^*_{5'5'} \sim 21$ kJ/gfw) corresponds to the fully inverse ($s_4 = 0$) limit of the extrapolated values of the configurational Gibbs energy for Fe_3O_4 obtained by Wu and Mason (1981) from their 600–1500 °C thermopower data (cf. Sack and Ghiorso, 1991, Fig. 3). The fact that these estimates converge at temperatures below the Curie point implies that Wu and Mason's interpretation of the physics of conduction of Fe_3O_4 at higher temperatures is in error. They assume that conduction proceeds exclusively by small polaron hopping between octahedral sites and ignore tetrahedral-tetrahedral, tetrahedral-octahedral, and octahedral-tetrahedral electron transfers. If their assumption becomes progressively more correct as Fe_3O_4 approaches the fully inverse, low temperature limit, then their calculated values for the configurational Gibbs energy should converge toward the correct value. This low temperature limiting value of the configurational Gibbs energy should correspond to the enthalpy of the ordering reaction implied by both the volume-composition systematics (Fig. 1) and the high temperature activity-composition constraints (Fig. 2), assuming that the parameters $\Delta\overline{S}^*_{5'5}$ and $W_{5'5}$ are negligible (cf. Sack and Ghiorso, 1991). We note that our revised value for the enthalpy of the Fe^{2+}-Fe^{3+} ordering reaction in Fe_3O_4 ($\Delta\overline{H}^*_{5'5} = 26.2$ kJ/gfw) results in an improved fit of data defining Fe-Ti exchange equilibria between rhombohedral oxides and spinels (e.g., Ghiorso, 1990a).

Because cation distributions in Fe_3O_4 are substantially inverse at all temperatures (e.g., Sack and Ghiorso, 1991), uncertainties in the ordering state such as those discussed in the previous paragraph do not have major effects on derived thermodynamic properties. The most noticeable consequence is in calculated miscibility gaps in spinel rich in $FeCr_2O_4$-Fe_3O_4. Small errors in the ordering state of Fe_3O_4 result in displacements of calculated miscibility gaps in spinel rich in $FeCr_2O_4$-Fe_3O_4 in the spinel prism (Figs. 8–10), toward slightly more symmetric compositions than those inferred from metamorphic assemblages (Loferski and Lipin, 1983; Zakrzewski, 1989). Such errors would contribute to uncertainties in the slopes of tie lines in two-phase regions and to uncertain temperatures of miscibility gaps. The latter cannot be inferred to be known to better than 20 °C given the uncertainties introduced by extrapolation of our model in temperature and our neglect of both defect equilibria and magnetic phenomena in formulating thermodynamic mixing properties (cf. Ghiorso, 1990b; Sack and Ghiorso, 1991; Ghiorso and Sack, 1991). [Magnetic interactions probably give rise to a miscibility gap in the Fe_2TiO_4-Fe_3O_4 binary at temperatures below the Curie point of magnetite (~573 °C). The effect has been demonstrated quantitatively in the analogous rhombohedral oxide system $FeTiO_3$-Fe_2O_3 (Burton and Davidson, 1988).] Uncertainties in the cation ordering states of 2–3 spinel end-members ($MgFe_2O_4$ and $MgAl_2O_4$) would be much more prohibitive to the development of a thermodynamic model for multicomponent spinels, as they display greater temperature dependence of their degree of cation order. For example, we have discovered that our model is sufficiently sensitive to the assumed ordering state of $MgAl_2O_4$ that a greater temperature dependence than that permitted by the tight constraints of Millard et al. (in preparation) and Peterson et al. (in preparation) would be problematic. If we were to employ the erronous temperature-ordering relations of Wood et al. (1986) for $MgAl_2O_4$, we could not, in detail, satisfy constraints on Fe-Mg partitioning (e.g., Figs. 5–7) without violating our assumption that the entropy of the

Fe-Mg exchange between olivine and aluminate spinels is negligible. A nonnegligible entropy would need to be invoked as a proxy for the incorrect description of the ordering state. Without creating such an entropy, optimizing agreement with high-temperature constraints on Fe-Mg partitioning in assemblages of olivine + aluminate-chromate spinel with the ordering description of Wood et al. (1986) would result in temperatures calculated from Equation 21 that are at least 50 °C too low to be consistent with the thermal decomposition of chlorite in the serpentinites considered by Evans and Frost (1975) (Fig. 7).

Last, it is unlikely that any uncertainty in the thermodynamic mixing properties of Fe-Mg olivine is a substantial contributing factor to errors in our model for the thermodynamic mixing properties of multicomponent spinels. We have amply developed arguments to the effect that the nonideality associated with mixing of Fe and Mg in $(Mg,Fe)_2SiO_4$ olivine must be at least about 5 kJ/gfw at intermediate ratios of Fe/(Fe + Mg) (e.g., Sack and Ghiorso, 1989, 1991). This study provides indirect confirmation of this inference. Our geothermometer based on the exchange of Mg and Fe between olivine and spinel (Eq. 21) successfully predicts temperatures for coexisting olivine and spinels that encompass the range of compositions encountered in nature and in the laboratory. It is more than coincidental that this feat has been accomplished for the physically plausible approximations that (1) the differences in vibrational entropies between the fully inverse Fe and Mg end-members are identical for the aluminate, ferrite, chromate, and titanate spinels (on a per atom Fe-Mg exchange basis) and (2) the vibrational entropies of all reciprocal, reciprocal-ordering, and exchange reactions are negligible.

Summary

We have developed a model for the thermodynamic properties of chromian spinels that is consistent with miscibility-gap features, standard-state properties, activity-composition relations, site-occupancy constraints, and Fe-Mg and Al-Cr partitioning relations between spinels and olivine, and spinels and corundum-eskaolaiite and $NaAlSi_2O_6$-$NaCrSi_2O_6$ solid solutions. This model is internally consistent with the thermodynamic data of Berman (1988) and the solution theory for olivine, orthopyroxenes, and rhombohedral oxides developed earlier (Sack and Ghiorso, 1989; Ghiorso, 1990a). We emphasize that this is the only context in which the model should be used. To facilitate application of our model to petrological problems, we have developed software to calculate equilibration temperatures for the Fe-Mg exchange between olivine + spinel assemblages (Eq. 21) and to compute activities of end-member components in spinels at specified temperatures and low pressures. The geothermometer and activity programs are available and may be obtained by anonymous FTP from internet node fondue.geology.washington.edu.

Acknowledgments

We would like to thank J.B. Thompson, Jr. for introducing us directly (R.O.S.) and indirectly (M.S.G.) to the mysteries and elegance of phase equilibrium in mineral solutions. Material support for this investigation was provided by the National Science Foundation through grants EAR-8451694 (M.S.G.) and EAR-8904270 (R.O.S.). Computations were facilitated by a generous equipment grant from Digital Equipment Corporation. We thank J.F. Allan and B.W. Evans for helpful discussions; J.F. Allan, C.R. Bina, B.R. Frost, and two anonymous reviewers for their constructive criticisms of an earlier draft; and J.F. Allan, R.L. Millard, and R.C. Peterson for sharing data in advance of publication.

References cited

Agrell, S.O., Boyd, F.R., Bunch, T.E., Cameron, E.N., Dence, M.R., Douglas, J.A.V., Haggerty, S.E., James, O.B., Keil, K., Peckett, A., Plant, A.G., Prinz, M., and Trail, R.J. (1970) Titanian chromite, aluminate and chromian ulvospinel from Apollo 11 rocks. Proceedings of the Apollo 11 Lunar Science Conference. Geochimica et Cosmochimica Acta, 1 (suppl. 1), 81–86.

Allan, J.F., Batiza, R., and Lonsdale, P. (1987) Petrology of lavas from seamounts flanking the East Pacific Rise axis, 21°N: Implications concerning the mantle source composition for both seamount and adjacent EPR lavas. In B. Keating, I. Fryer, R. Batiza, and G.W. Boehlert, Eds., Seamounts, islands, and atolls, p. 255–282. American Geophysical Union Monograph Series, Washington, D.C.

Allan, J.F., Sack, R.O., and Batiza, R. (1988) Cr-rich spinels as petrogenetic indicators: MORB-type lavas from the Lamont seamount chain, Eastern Pacific. American Mineralogist, 73, 741–753.

Allan, J.F., Batiza, R., Perfit, M.R., Fornari, D.J., and Sack, R.O. (1989) Petrology of lavas from the Lamont seamount chain and adjacent East Pacific Rise, 10°N. Journal of Petrology, 30, 1245–1298.

Banerjee, S.K., O'Reilly, W., Gibb, T.C., and Greenwood, N.N. (1967) The behavior of ferrous ions in iron-titanium spinels. Journal of Physics and Chemistry of Solids, 28, 1323–1335.

Berman, R.G. (1988) Internally-consistent thermodynamic data for minerals in the system Na_2O-K_2O-CaO-MgO-FeO-Fe_2O_3-Al_2O_3-SiO_2-TiO_2-H_2O-CO_2. Journal of Petrology, 29, 445–522.

Berman, R.G., and Brown, T.H. (1985) Heat capacities of minerals in the system Na_2O-K_2O-CaO-MgO-FeO-Fe_2O_3-Al_2O_3-SiO_2-TiO_2-H_2O-CO_2: Representation, estimation, and high temperature extrapolation. Contributions to Mineralogy and Petrology, 89, 168–183.

Burton, B.P., and Davidson, P.M. (1988) Multicritical phase relations in minerals. In S. Ghose, J.M.D. Coey, and E. Salje, Eds., Structural and magnetic phase transitions in minerals, p. 60–90. Springer-Verlag, New York.

Carroll Webb, S.A., and Wood, B.J. (1986) Spinel-pyroxene-garnet relationships and their dependence on Cr/Al ratio. Contributions to Mineralogy and Petrology, 92, 471–480.

Champness, P.E., Dunham, A.C., Gibb, F.G.F., Giles, H.N., MacKenzie, W.S., Stumpfl, E.F., and Zussman, J. (1971) Mineralogy and petrology of some Apollo 12 lunar samples. Proceedings of the Second Lunar Science Conference. Geochimica et Cosmochimica Acta, 1 (suppl. 1), 359–376.

Chatterjee, N.D., Leistner, H., Terhart, L., Abraham, K., and Klaska, R. (1982) Thermodynamic mixing properties of corundum-eskaolaiite, α-$(Al,Cr^{3+})_2O_3$, crystalline solutions at high temperatures and pressures. American Mineralogist, 67, 725–735.

Cremar, V. (1969) Die Mischkristallbildung im System Chromit-Magnetit-Hercynit zwischen 1000 °C und 500 °C. Neues Jahrbuch für Mineralogie Abhandlungen, 111, 184–205.

Darken, L.S., and Gurry, R.W. (1953) Physical chemistry of metals, 535 p. McGraw-Hill, New York.

Dunitz, J.D., and Orgel, L.E. (1957) Electronic properties of transition metal oxides II. Journal of the Physics and Chemistry of Solids, 3, 318–323.

Ebel, D.S., and Sack, R.O. (1989) Ag-Cu and As-Sb exchange energies in tetrahedrite-tennantite fahlores. Geochimica et Cosmochimica Acta, 53, 2301–2309.

El Goresy, A. (1976) Oxide minerals in lunar rocks. In D. Rumble III, Ed., Oxide minerals, p. EG-1–EG-45. Mineralogical Society of America Short Course Notes, Washington, DC.

Engi, M. (1983) Equilibria involving Al-Cr spinel: Mg-Fe exchange with olivine. Experiments, thermodynamic analysis, and consequences of geothermometry. American Journal of Science, 283A, 29–71.

Evans, B.W., and Frost, B.R. (1975) Chrome-spinel in progressive metamorphism—a preliminary analysis. Geochimica et Cosmochimica Acta, 39, 959–972.

Evans, B.W., and Moore, R.G. (1968) Mineralogy as a function of depth in the prehistoric Makaopuhi tholeiitic lava lake. Contributions to Mineralogy and Petrology, 17, 85–115.

Francombe, M.H. (1957) Lattice changes in spinel-type iron chromites. Journal of Physics and Chemistry of Solids, 3, 37–43.

Gee. L.L., and Sack, R.O. (1988) Experimental petrology of melilite nephelinites. Journal of Petrology, 29, 1233–1255.

Ghiorso, M.S. (1990a) Thermodynamic properties of hematite-ilmenite-geikielite solid solutions. Contributions to Mineralogy and Petrology, 104, 645–667.

——— (1990b) A note on the application of the Darken equation to mineral solid solutions with variable degrees of order-disorder. American Mineralogist, 75, 539–544.

Ghiorso, M.S., and Sack, R.O. (1991) Fe-Ti oxide geothermometry: Thermodynamic formulation and the estimation of intensive variables in silicic magmas. Contributions to Mineralogy and Petrology, in press.

Gopal, E.S.R. (1966) Specific heats at low temperatures, 240 p. Plenum Press, New York.

Haggerty, S.E., and Meyer, H.O.A. (1970) Apollo 12: Opaque oxides. Earth and Planetary Science Letters, 9, 379–387.

Hill, R.L., and Sack, R.O. (1987) Thermodynamic properties of Fe-Mg titaniferous magnetite spinels. Canadian Mineralogist, 25, 443–464.

Hoffman, M.A., and Walker, D. (1978) Textural and chemical variations of olivine and chrome spinel in the East Dover ultramafic bodies, south-central Vermont. Geological Society of America Bulletin, 89, 699–710.

Indolev, L.N., Nevoysa, I.A., and Bryzgalov, I.A. (1971) New data on the composition of stibnite and the isomorphism of copper and silver. Doklady Akademii Nauk SSSR, 199, 115–118.

Irvine, T.N. (1965) Chromium spinel as a petrogenetic indicator. Part I. Theory. Canadian Journal of Earth Sciences, 2, 648–672.

——— (1967) Chromium spinel as a petrogenetic indicator. Part II. Petrological applications. Canadian Journal of Earth Sciences, 4, 71–103.

Jacob, K.T. (1978) Electrochemical determination of activities in Cr_2O_3-Al_2O_3 solid solutions. Journal of the Electrochemical Society, 125, 175–179.

Jamieson, H.E., and Roeder, P.L. (1984) The distribution of Mg and Fe^{2+} between olivine and spinel at 1300 °C. American Mineralogist, 69, 283–291.

Katsura, T., Wakihara, M., Shin-Ichi, H., and Sugihara, T. (1975) Some thermodynamic properties in spinel solid solutions with the Fe_3O_4 component. Journal of Solid State Chemistry, 13, 107–113.

King, E.G. (1954) Heat capacities at low temperatures and entropies at 298.15°K. of crystalline calcium and magnesium ferrites. Journal of the American Ceramic Society, 76, 5849–5850.

——— (1955) Heat capacities at low temperatures and entropies at 298.15°K. of crystalline calcium and magnesium aluminates. Journal of Physical Chemistry, 59, 218–219.

——— (1956) Heat capacities at low temperatures and entropies of five spinel minerals. Journal of Physical Chemistry, 60, 410–412.

Lehmann, J., and Roux, J. (1986) Experimental and theoretical study of (Fe^{2+},Mg) $(Al,Fe^{3+})_2O_4$ spinels: Activity-composition relationships, miscibility gaps, vacancy contents. Geochimica et Cosmochimica Acta, 50, 1765–1783.

Loferski, P.J., and Lipin, B.R. (1983) Exsolution in metamorphosed chromite from the Red Lodge district, Montana. American Mineralogist, 68, 777–789.

McGuire, T.R. Howard, L.N., and Smart, J.S. (1952) Magnetic properties of the chromites. Ceramic Age, 60, 22–24.

Muan, A., Hauck, J., and Lofall, T. (1972) Equilibrium studies with a bearing on lunar rocks. Proceedings of the Third Lunar Science Conference. Geochimica et Cosmochimica Acta, 1 (suppl. 1), 185–196.

Muir, J.E., and Naldrett, A.J. (1973) A natural occurrence of two-phase chromium-bearing spinels. Canadian Mineralogist, 11, 930–939.

Murck, B.W., and Campbell, I.H. (1986) The effects of temperature, oxygen fugacity and melt composition on the behavior of chromium in basic and ultrabasic melts. Geochimica et Cosmochimica Acta, 50, 1871–1887.

Navrotsky, A., and Kleppa, O.J. (1967) The thermodynamics of cation distributions in simple spinels. Journal of Inorganic and Nuclear Chemistry, 30, 479–498.

Naylor, B.F. (1944) High-temperature heat contents of ferrous and magnesium chromites. Industrial and Engineering Chemistry, 36, 933–934.

Oka, Y., Steinke, P., and Chatterjee, N.D. (1984) Thermodynamic mixing properties of $Mg(Al,Cr)_2O_4$ spinel crystalline solution at high temperatures and pressures. Contributions to Mineralogy and Petrology, 87, 197–204.

O'Leary, M.J., and Sack, R.O. (1987) Fe-Zn exchange reaction between tetrahedrite and sphalerite in natural environments. Contributions to Mineralogy and Petrology, 96, 415–425.

Paar, Von, W.H., Chen, T.T., and Cunther, W. (1978) Extreme silber-reicher Freibergit in Pb-Zn-Cu-Erzen des Bergbaues "Knappenstube," Hoctor, Salzburg. Carinthia II, 168, 35–42.

Parker, V.B., Wagman, D.D., and Evans, W.H. (1971) Selected values of chemical thermodynamic properties. National Bureau of Standards Technical Note, 270-6, 106 p.

Petric, A., and Jacob, K.T. (1982a) Thermodynamic properties of Fe_3O_4-FeV_2O_4 and Fe_3O_4-$FeCr_2O_4$ spinel solid solutions. Journal of the American Ceramic Society, 65, 117–123.

——— (1982b) Inter- and intra-crystalline ion-exchange equilibria in the system Fe-Cr-Al-O. Solid State Ionics, 6, 47–56.

Riley, J.F. (1974) The tetrahedrite-freibergite series, with reference to the Mount Isa Pb-Zn-Ag ore body. Mineralium Deposita, 9, 117–124.

Robbins, M., Wertheim, G.K., Sherwood, R.C., and Buchanan, D.N.E. (1971) Magnetic properties and site distributions in the system $FeCr_2O_4$-Fe_3O_4 ($Fe^{2+}Cr_{2-x}Fe_x^{3+}O_4$). Journal of Physics and Chemistry of Solids, 32, 717–729.

Robie, R.A., Hemingway, B.S., and Fisher, J.R. (1978) Thermodynamic properties of minerals and related substances at 298.15 K and 1 bar (10^5 Pascals) pressure and at higher temperatures. Geological Society of America Bulletin, 1452, 456 p.

Sack, R.O. (1982) Spinels as petrogenetic indicators: Activity-composition relations at low pressures. Contributions to Mineralogy and Petrology, 79, 169–182.

——— (1991) Thermochemistry of tetrahedrite-tennantite fahlores. In N.L. Ross and G.D. Price, Eds. The stability of minerals. Harper Collins Academic, London (in press).

Sack, R.O., and Ghiorso, M.S. (1989) Importance of considerations of mixing properties in establishing an internally consistent thermodynamic database: Thermochemistry of minerals in the system Mg_2SiO_4-Fe_2SiO_4-SiO_2. Contributions to Mineralogy and Petrology, 102, 41–68.

——— (1991) An internally consistent model for the thermodynamic properties of Fe-Mg-titanomagnetite-aluminate spinels. Contributions to Mineralogy and Petrology, 106, 474–505.

Sack, R.O., Ebel, D.S., and O'Leary, M.J. (1987a) Tennahedrite thermochemistry and metal zoning. In H.C. Helgeson, Ed., Chemical transport in metasomatic processes, p. 701–731. Reidel, Dordrecht, The Netherlands.

Sack, R.O., Walker, D., and Carmichael, I.S.E. (1987b) Experimental petrology of alkalic lavas: Constraints on cotectics of multiple saturation in natural basic liquids. Contributions to Mineralogy and Petrology, 96, 1–23.

Shaked, H., Hastings, J.M., and Corliss, L.M. (1970) Magnetic structure of magnesium chromite. Physical Review B, 7, 3116–3124.

Sharma, K.K., Langer, K., and Sieffert, T. (1973) Some properties of spinel phases in the binary system $MgAl_2O_4$-$MgFe_2O_4$. Neues Jahrbuch für Mineralogie Mitteilungen, 442–449.

Shearer, J.S., and Kleppa, O.J. (1973) The enthalpies of formation of $MgAl_2O_4$, $MgSiO_3$, Mg_2SiO_4 and Al_2SiO_5 by oxide melt solution calorimetry. Journal of Inorganic and Nuclear Chemistry, 35, 1073–1078.

Shirane, G., Cox, D.E., and Pickart, S.J. (1964) Magnetic structures in $FeCr_2S_4$ and $FeCr_2O_4$. Journal of Applied Physics, 35, 954–955.

Shishkov, V.I., Lykasov, A.A., and Il'ina, A.F. (1980) Activity of the components of iron-magnesium spinel. Russian Journal of Physical Chemistry, 54, 440–441.

Shomate, C.H. (1944) Ferrous and magnesium chromites. Specific heats at low temperatures. Industrial and Engineering Chemistry, 36, 910–911.

Spiridonov, E.M. (1984) Species and varieties of fahlore (tetrahedrite-tennantite) minerals and their rational nomenclature. Doklady Akademii Nauk SSSR, 279, 166–172.

Stull, D.R., and Prophet, H. (1971) JANAF thermochemical tables (2nd edition). National Bureau of Standards Reference Data Series (NBS) NSRDS-NBS 37, 1141 p.

Taylor, L.A., Kullerud, G., and Bryan, W.B. (1971) Opaque mineralogy and textural features of Apollo 12 samples and a comparison with Apollo 11 rocks. Proceedings of the Second Lunar Science Conference, 855–871.

Thompson, J.B., Jr. (1969) Chemical reactions in crystals. American Mineralogist, 54, 341–375.

Todd, S.S., and King, E.G. (1953) Heat capacities at low temperature and entropies at 298.16°K. of titanomagnetite and ferric titanate. Journal of the American Ceramic Society, 75, 4547–4549.

Trinel-Dufour, M.C., and Perrot, P. (1977) Etude thermodynamique des solution solides dans le systeme Fe-Mg-O. Annale Chimie, 2, 309–318.

Turnock, A.C., and Eugster, H.P. (1962) Fe-Al oxides; phase relationships below 1000 °C. Journal of Petrology, 3, 533–565.

Wagman, D.D., Evans, W.H., Parker, V.B., Halow, I., Bailey, S.M., and Schumm, R.H. (1969) Selected values of chemical thermodynamic properties. National Bureau of Standards Technical Note, 270–4, 152 p.

Wechsler, B.A., and Navrotsky, A. (1984) Thermodynamics and structural chemistry of compounds in the system MgO-TiO_2. Journal of Solid State Chemistry, 55, 165–180.

Westrum E.F., Jr, and Grønvold, F. (1969) Magnetite (Fe_3O_4) heat capacity and thermodynamic properties from 5 to 350 K, low temperature transition. Journal of Chemical Thermodynamics, 1, 543–557.

Wood, B.J., Kirkpatrick, R.J., and Montez, B. (1986) Order-disorder phenomena in $MgAl_2O_4$ spinel. American Mineralogist, 71, 999–1006.

Wu, C.C., and Mason, T.O. (1981) Thermopower measurement of cation distribution in magnetite. Journal of the American Ceramic Society, 64, 520–552.

Zakrzewski, M.A. (1989) Chromian spinels from Kusså, Bergslagen, Sweden. American Mineralogist, 74, 448–455.

Manuscript received January 30, 1990
Manuscript accepted February 25, 1991